



Article

Dynamics of the Ligand Excited States Relaxation in Novel β -Diketonates of Non-Luminescent Trivalent Metal Ions

Trofim Polikovskiy ¹, Vladislav Korshunov ¹, Victoria Gontcharenko ^{1,2} , Mikhail Kiskin ³ , Yuriy Belousov ^{1,4} , Claudio Pettinari ⁵ and Ilya Taydakov ^{1,*}

¹ P. N. Lebedev Physical Institute of the Russian Academy of Sciences, 53 Leninsky 1. Prospect, 119991 Moscow, Russia

² Faculty of Chemistry, National Research University Higher School of Economics, 20 Miasnitskaya Str., 101000 Moscow, Russia

³ Kurnakov Institute of General and Inorganic Chemistry, Russian Academy of Sciences, 119991 Moscow, Russia

⁴ Chemistry Department, M. V. Lomonosov Moscow State University, Leninskie Gory Str, Building 1/3, 119991 Moscow, Russia

⁵ Chemistry Interdisciplinary Project (ChIP), School of Pharmacy, University of Camerino, Via Madonna delle Carceri, 62032 Camerino, Italy

* Correspondence: ivt@lebedev.ru

Abstract: Complexes emitting in the blue spectral region are attractive materials for developing white-colored light sources. Here, we report the luminescence properties of novel coordination compounds based on the trivalent group 3, 13 metals, and the 1-phenyl-3-methyl-4-cyclohexylcarbonyl-pyrazol-5-one (Q^{CH}) ligand. $[M(Q^{CH})_3]$ ($M = Al, Ga, \text{ and } In$), $[M(Q^{CH})_3(H_2O)]$ ($M = Sc, Gd, \text{ and } Lu$), $[Lu(Q^{CH})_3(DMSO)]$, and $[La(Q^{CH})_3(H_2O)(EtOH)]$ complexes were synthesized and structurally characterized by a single-crystal X-ray diffraction study. It has been found that the luminescence quantum yields of the ligand increase by one order of magnitude upon metal coordination. A significant correspondence between the energies of the ligand's excited states and the luminescence quantum yields to the metal ion's atomic numbers was found using molecular spectroscopy techniques. The replacement of the central ion with the heavier one leads to a monotonic increase in singlet state energy, while the energy of the triplet state is similar for all the complexes. Time-resolved measurements allowed us to estimate the intersystem crossing (ISC) rate constants. It was shown that replacing the Al^{3+} ion with the heavier diamagnetic Ga^{3+} and In^{3+} ions decreased the ISC rate, while the replacement with the paramagnetic Gd^{3+} ion increased the ISC rate, which resulted in a remarkably bright and room-temperature phosphorescence of $[Gd(Q^{CH})_3(H_2O)]$.

Keywords: luminescence; lanthanides; rare earths; coordination compounds; 1,3-diketones; 4-acylpyrazolones; aluminum; gallium; indium



Citation: Polikovskiy, T.; Korshunov, V.; Gontcharenko, V.; Kiskin, M.; Belousov, Y.; Pettinari, C.; Taydakov, I. Dynamics of the Ligand Excited States Relaxation in Novel β -Diketonates of Non-Luminescent Trivalent Metal Ions. *Int. J. Mol. Sci.* **2023**, *24*, 8131. <https://doi.org/10.3390/ijms24098131>

Academic Editor: Oleg V. Mikhailov

Received: 3 April 2023

Revised: 26 April 2023

Accepted: 27 April 2023

Published: 1 May 2023



Copyright: © 2023 by the authors. Licensee MDPI, Basel, Switzerland. This article is an open access article distributed under the terms and conditions of the Creative Commons Attribution (CC BY) license (<https://creativecommons.org/licenses/by/4.0/>).

1. Introduction

White organic light-emitting diodes (WOLEDs) are the most economical light sources for street, home, and display lighting and many other special applications [1–3]. White emissions in such devices are conditioned by simultaneous emissions of several luminophores in blue, green, and red spectral areas [2], providing an R-G-B scheme of white light [3], or emissions of blue and orange emitters, providing a B-O scheme. One of the most popular classes of materials used in WOLEDs are the platinum-based group materials, especially those based on Ir(III) complexes containing 2-phenylpyridine fluorinated derivatives and imidazole-type carbene compounds [4,5]. The commercial price of production of such materials is relatively high, which makes the technology quite expensive [6].

An attractive class of blue light-emitting materials is formed by small organic molecules, such as triarylboranes and triarylmethanes [7,8]. A great interest has arisen in recent years

for a wide range of such compounds and a variety of approaches for changing photophysical properties by small variations in the chemical structure has been reported [9]. Among these compounds, β -diketones are noteworthy molecules due to the possibility of fine-tuning the energy of first excited singlet (S_1) and triplet (T_1) states and their potential application in OLEDs [10,11]. Furthermore, phosphorescence or even thermally activated delayed fluorescence (TADF) can be achieved in some cases [12]. However, β -diketones often have critically low emission quantum yields due to several non-radiative relaxation processes, in particular, vibration multiphonon relaxation on O-H and C-H oscillators [13]. Keto-enol tautomerism makes the energy relaxation dynamic more complicated due to excited state intermolecular proton transfer (ESIPT), which is associated with proton localization near the diketone oxygen atom [14]. This limits the luminescence efficiency of diketone derivatives. Luckily, the luminescence performance of β -diketones can be dramatically improved by the formation of metal complexes. When β -diketonates are coordinated to metal, they exist exclusively in the enolic form and consequently, a significant increase in the luminescence quantum yield is observed [9,15].

On the other hand, luminescence efficiency can be adjusted by changing the energies of S_1 and T_1 as well as the excited states' lifetimes [16–18]. There are many studies aimed at the investigation of the dependence of these photophysical properties on minor chemical structure change [19–21].

Notably, there is currently no general theory describing how photophysical properties of a ligand change upon coordination to different metal ions. Several empirically derived guidelines enable a prediction of the energy change in the first excited singlet state [22], the triplet state [23], or the luminescence quantum yield [24]. According to these rules, we can estimate the luminescence efficiency of coordination compounds. However, such rules are rather imprecise, and there are many exceptions to them [25]. In addition, no systematic study has been reported on the role of the metal ion in coordination compounds on the energies of excited ligand states, on the energy transfer processes, and, consequently, on the luminescence quantum yield.

Among all the β -diketonate ligands, 4-acylpyrazolonates must be highlighted due to their outstanding properties [26–28], such as their sufficient chemical and thermal stability, comparably effortless chemical synthesis, and relatively high energy of the first excited triplet state T_1 , which can range from 21,000 to 24,000 cm^{-1} depending on the ligand substituents [29–36].

The spectroscopic characteristics of β -diketonate complexes, i.e., the luminescence quantum yields and the excited state's lifetime unpredictably depend on the nature of the metal. Thus, typical f-elements, such as Eu^{3+} , Tb^{3+} , Dy^{3+} , and Sm^{3+} , as well as some IR-emitting ions, luminesce mainly due to the antenna sensitization mechanism [37]. For rhenium and platinum metal complexes, the metal orbitals play an important part in the electronic transitions that cause luminescence [4,5]. At the same time, cations with an electronic configuration, such as that of noble gases, i.e., Al^{3+} , Ga^{3+} , In^{3+} , Sc^{3+} , and La^{3+} (as well as the Lu^{3+} ion, which has the electronic configuration $[\text{Xe}]4f^{14}$), influence the ligand luminescence not through the internal electronic transitions or the participation of valence orbitals, but only by changing the ligand space structure and by influencing the charge field on it. They are usually characterized by fluorescence with low lifetimes, and the emission color, depending on the ligand, lies in the violet-blue region [38]. The Gd^{3+} ion may exhibit its own 4f-f electronic transitions, but due to the high resonance level energy ($>30,000 \text{ cm}^{-1}$) [37] and paramagnetism-related effects, gadolinium complexes are characterized by phosphorescence in the blue-green spectral region [39].

To date, among the thirteen group metals (Al, Ga, and In), only one Ga^{3+} acylpyrazolonate complex has been described [40]. While aluminum compounds (such as 8-oxyquinolate [41]) have played a crucial role in the history of OLED technology, the lack of research on group 13 acylpyrazolonates poses a certain challenge.

Corresponding lanthanide derivatives have been widely investigated, but in most of cases the attention has been paid on the luminescence properties of emitting f-elements, mainly terbium and europium [27,28].

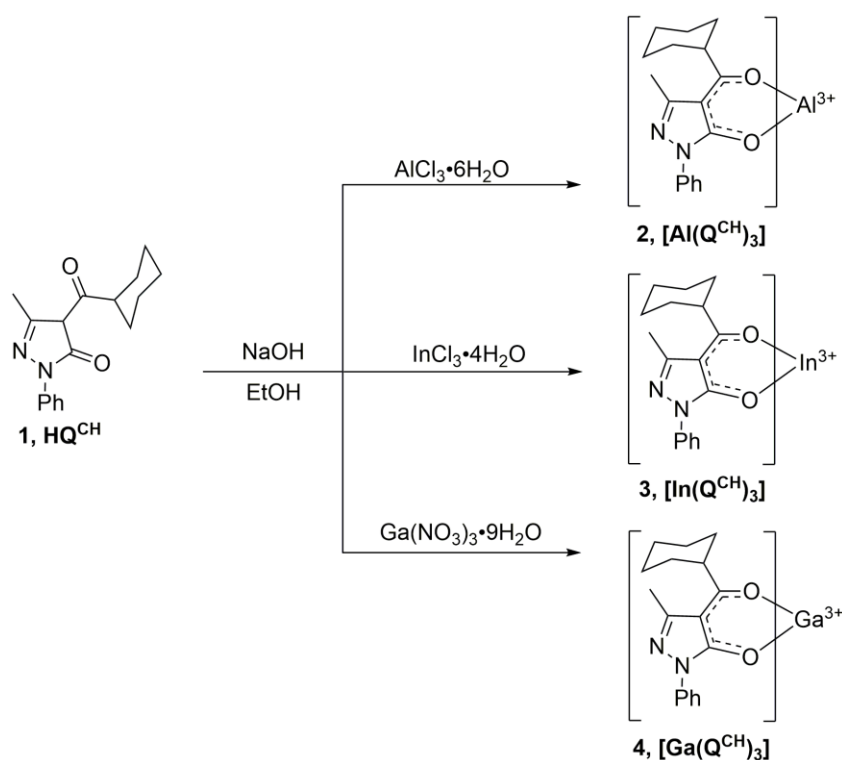
Here, we report two series of coordination compounds obtained from the reaction of the trivalent metals, i.e., the 13 group metals (Al^{3+} , Ga^{3+} , and In^{3+}), 3 group metals (Sc^{3+} , La^{3+} , Gd^{3+} , and Lu^{3+}), and the proligand 4-(cyclohexanecarbonyl)-5-methyl-2-phenyl-2,4-dihydro-3H-pyrazol-3-one HQ^{CH} , with the aim of qualitatively and quantitatively correlating the photophysical ligand parameters to the central ion choice. We select this ligand since it allows the synthesis of compounds containing ions of various radii from Al^{3+} to Lu^{3+} . Earlier, we showed that Q^{CH} lanthanide complexes exhibit excellent luminescent properties [42,43], and that the cyclohexyl substituent prevents the formation of molecular aggregates due to the molecular volume [44].

In order to disclose the influence of different metal ions on the ligand's electronic structure, we also investigated in detail the photophysical properties of all the complexes by exploring the absorption, excitation, emission spectra, quantum yields of luminescence, and the lifetime of the excited states. All of the complexes reported here exhibit strong emissions in the blue-green region of the spectra, which makes them promising for use as blue emitting layer components in WOLEDs.

2. Results

2.1. Synthesis of Complexes

The complexes $[\text{M}(\text{Q}^{\text{CH}})_3]$ 2–4 ($\text{M} = \text{Al}$, Ga , and In) of all the three elements can be readily prepared in high yields in aqueous EtOH media, using hydrated salts as the metal precursors and NaOH as the base (Scheme 1):

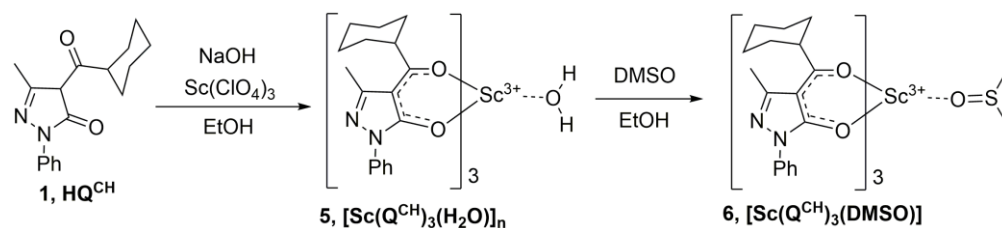


Scheme 1. Preparation of Al^{3+} , Ga^{3+} , and In^{3+} complexes (2–4).

All three complexes were obtained in an anhydrous form and can be purified by recrystallization from hot EtOH. Gallium (III) nitrate was used as a source of Ga^{3+} ion as it is the most soluble salt. The nature of the anion did not affect the yield of the complexes.

It is worth noting that the Al^{3+} , Ga^{3+} , and In^{3+} complexes containing acylpyrazolonates have been scarcely studied to date [26]. Several aluminum complexes have been previously obtained from the interaction of $\text{Al}(\text{i-PrO})_3$ or anhydrous AlCl_3 with three different 4-acylpyrazolones-5, bearing 4-acetyl, 4-benzyl, or 4-propionyl fragments in benzene [45]. Analogous In^{3+} complexes were prepared using $\text{In}(\text{i-PrO})_3$ as the starting material with a method also employed for the preparation of Al^{3+} ion complexes [46]. Al^{3+} and In^{3+} ion derivatives of 1-phenyl-3-methyl-4-trifluoroacetyl-pyrazolonate [47] and a binuclear In^{3+} complex with the multitopic 1,10-bis(1-phenyl-3-methyl-5-hydroxy-4-pyrazolyl)-1,10-decanedionate were synthesized and investigated in the extraction of indium and aluminum from the solutions [48]. Only $\text{Ga}(\text{1-phenyl-3-methyl-4-benzoyl-pyrazolonate})$ was reported in the literature without a detailed description of its preparation [49].

The interaction of HQ^{CH} (1) with $\text{Sc}(\text{ClO}_4)_3$ and NaOH in the $\text{EtOH-H}_2\text{O}$ mixture led to the formation of $[\text{Sc}(\text{Q}^{\text{CH}})_3(\text{H}_2\text{O})]_n$ (5), as it was confirmed by an EA and FTIR data. This complex is insoluble in most solvents, including alcohols, which may testify to its polymeric structure with bridge water molecules. Previously, we have shown that for Sc^{3+} diketonates with heterocyclic ligands, a coordination number (CN) equal to seven is preferable [15]. This complex is readily soluble in coordinating solvents, such as DMSO, upon gentle heating. A ligand exchange occurs due to dissolution with the formation of a monomeric species (Scheme 2).

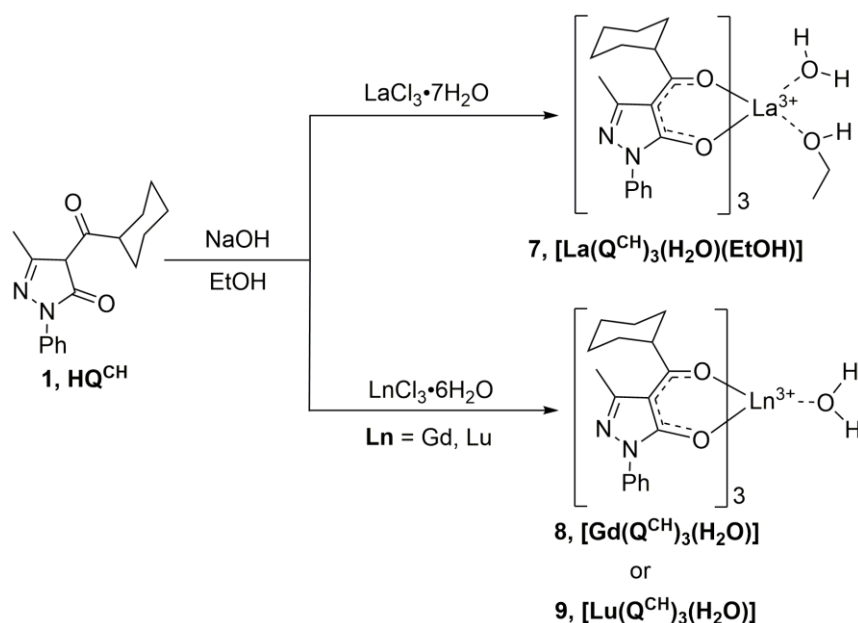


Scheme 2. Preparation of Sc^{3+} complexes.

Notably, upon the slow diffusion of EtOH vapor into a saturated DMSO solution of $[\text{Sc}(\text{Q}^{\text{CH}})_3(\text{H}_2\text{O})]_n$ (5) fine crystals of $[\text{Sc}(\text{Q}^{\text{CH}})_3(\text{DMSO})]$ (6), a complex formed as a sole product due to the higher coordination ability of DMSO over EtOH . The choice of $\text{Sc}(\text{ClO}_4)_3$ is not critical for the synthesis; other soluble salts, such as chlorides or nitrates, can be used. However, it is more convenient to dissolve Sc_2O_3 in non-volatile HClO_4 rather than in HCl or HNO_3 .

For scandium (III), only one complex with 1-phenyl-3-methyl-4-benzoyl-pyrazolone-5 (HL_1) was reported [50]. It was obtained by an interaction between the free ligand, hydrated $\text{Sc}(\text{NO}_3)_3$ in MeOH without a base, and identified as $[\text{Sc}(\text{L}_1)_3] \cdot \text{H}_2\text{O}$ on the basis of an elemental analysis (EA) and FTIR data. Upon crystallization from hot MeOH , this amorphous complex transformed into anhydrous crystalline $[\text{Sc}(\text{L}_1)_3]$, but no crystal structure data were provided. Complexes of La^{3+} and Lu^{3+} ions were obtained by a modified method, which has been described previously in the literature for other lanthanides [42,51,52] (Scheme 3).

Since the ionic radius of La^{3+} is bigger than that of Lu^{3+} due to lanthanide contraction, La^{3+} demonstrates a higher CN (8) and adopts two additional ligands (EtOH and water molecules) alongside three bulky diketonate anions. For the Gd^{3+} ion and especially Lu^{3+} , the ion coordination number is 7, and only one additional water molecule can be inserted in the inner sphere of the complex together with three anions of Q^{CH} ligands. From hot EtOH complex $[\text{La}(\text{Q}^{\text{CH}})_3(\text{H}_2\text{O})(\text{EtOH})]$ (7) crystallized as a solvate with one molecule of EtOH , but it can be fully desolvated by heating at 45°C at a diminished pressure.



Scheme 3. Preparation of La^{3+} , Gd^{3+} , and Lu^{3+} complexes (7–9).

2.2. Single-Crystal X-ray Structures

2.2.1. Complexes with p-Metals

Pale brown crystals of complexes $[\text{Al}(\text{Q}^{\text{CH}})_3]$ (2), $[\text{In}(\text{Q}^{\text{CH}})_3]$ (3) and $[\text{Ga}(\text{Q}^{\text{CH}})_3]$ (4), which are suitable for single-crystal X-ray diffraction, were obtained by the slow evaporation of solutions in MeOH or EtOH at room temperature. The selected crystal data and refinement parameters for complexes $[\text{Al}(\text{Q}^{\text{CH}})_3]$, $[\text{Ga}(\text{Q}^{\text{CH}})_3]$, and $[\text{In}(\text{Q}^{\text{CH}})_3]$ are listed in Table 1. The isostructurality of single-crystals to polycrystalline bulk samples was confirmed by the powder X-ray diffraction method (PXRD) (Figures S1–S3).

Table 1. Crystal data and refinement parameters for $[\text{Al}(\text{Q}^{\text{CH}})_3]$, $[\text{Ga}(\text{Q}^{\text{CH}})_3]$, and $[\text{In}(\text{Q}^{\text{CH}})_3]$ (2–4).

| Parameter | $[\text{Al}(\text{Q}^{\text{CH}})_3]$ | $[\text{Ga}(\text{Q}^{\text{CH}})_3]$ | $[\text{In}(\text{Q}^{\text{CH}})_3]$ |
|-------------------|--|--|--|
| Molecular Formula | $\text{C}_{51}\text{H}_{56}\text{AlN}_6\text{O}_6$ | $\text{C}_{51}\text{H}_{56}\text{GaN}_6\text{O}_6$ | $\text{C}_{51}\text{H}_{56}\text{InN}_6\text{O}_6$ |
| M | 875.99 | 918.73 | 964.84 |
| Temperature, K | 100(2) | 110(2) | 100(2) |
| System | Monoclinic | Monoclinic | Triclinic |
| Space group | $\text{P}2_1/c$ | $\text{P}2_1/c$ | $\text{P}-1$ |
| a, Å | 17.9838(8) | 17.865(4) | 13.2087(14) |
| b, Å | 13.0521(6) | 12.918(3) | 20.270(2) |
| c, Å | 19.8671(9) | 20.037(4) | 20.561(3) |
| α , deg. | 90 | 90 | 110.542(5) |
| β , deg. | 92.303(2) | 92.95(3) | 93.380(5) |

Table 1. *Cont.*

| Parameter | [Al(Q ^{CH}) ₃] | [Ga(Q ^{CH}) ₃] | [In(Q ^{CH}) ₃] |
|--|---|---|---|
| γ , deg. | 90 | 90 | 108.234(4) |
| V , Å ³ | 4659.6(4) | 4618.3(16) | 4807.3(10) |
| Z | 4 | 4 | 4 |
| ρ_{calc} , g/cm ³ | 1.249 | 1.321 | 1.333 |
| $\mu(\text{MoK}\alpha)$, mm ⁻¹ | 0.100 | 0.653 | 0.546 |
| $F(000)$ | 1860 | 1932 | 2008 |
| $\theta_{\text{min}}-\theta_{\text{max}}$, deg. | 1.87–25.00 | 2.04–26.00 | 1.64–26.00 |
| Number of measured reflections | 32,091 | 31,594 | 54,548 |
| Number of unique reflections (R_{int}) | 8200 (0.0742) | 9059 (0.0633) | 18,843 (0.0792) |
| Number of reflections with $I > 2\sigma(I)$ | 5427 | 6154 | 13,863 |
| Number of refined parameters | 568 | 556 | 1159 |
| R-factors ($I > 2\sigma(I)$) | $R_1 = 0.1117$, $\omega R_2 = 0.2928$ | $R_1 = 0.1049$, $\omega R_2 = 0.2757$ | $R_1 = 0.0627$, $\omega R_2 = 0.1397$ |
| R-factors (all reflections) | $R_1 = 0.1499$, $\omega R_2 = 0.3274$ | $R_1 = 0.1414$, $\omega R_2 = 0.3028$ | $R_1 = 0.0914$, $\omega R_2 = 0.1566$ |
| GOOF | 1.026 | 1.052 | 1.021 |
| $\Delta\rho_{\text{max}}/\Delta\rho_{\text{min}}$, e/Å ³ | 1.534/−0.557 | 1.743/−0.941 | 1.999/−0.883 |

All three structures are mononuclear complexes, where the metal ion is coordinated by three diketonate ligands (Figures 1 and 2), and according to the CCDC analysis, these structures present the first example of such complexes of Al³⁺, Ga³⁺, and In³⁺ ions with β -diketones. It must be noted that the asymmetric unit of the [In(Q^{CH})₃] (3) crystal structure contains two molecules of the complex (Figure 2). Each central ion (Al³⁺, Ga³⁺, and In³⁺) bonds with two oxygen atoms of each ligand, leading to the octahedral coordination polyhedron {MO₆} and neutral charge of the complexes. As for the {InO₆} polyhedron, moderate distortion of the angle between two vertices can be observed, leading the O1-In1-O6 and O7-In2-O9 angles to be 171.2 and 173.2° instead of 180° for the ideal octahedron. The elongation of M-O bonds (Table S1) is observed for complexes [Al(Q^{CH})₃], [Ga(Q^{CH})₃], and [In(Q^{CH})₃], which is attributed to the increase in the ionic radius of the central metal ion. The analysis of crystal packing revealed no presence of any hydrogen bonds, but the presence of rather weak C-H... π was observed.

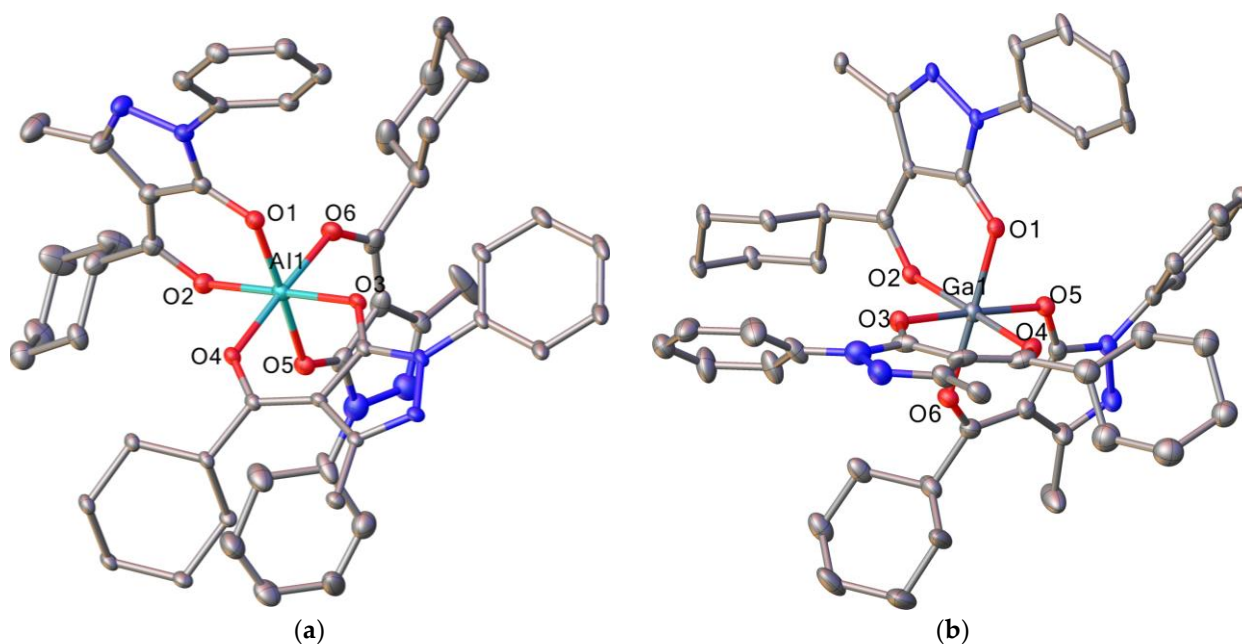


Figure 1. View of the asymmetric unit of $[\text{Al}(\text{Q}^{\text{CH}})_3]$ (a) and $[\text{Ga}(\text{Q}^{\text{CH}})_3]$ (b). Hydrogen atoms are not shown for clarity. Thermal ellipsoids are illustrated at 30% probability. Central metal atoms and oxygen atoms of ligands are labeled. Atoms are marked by colors as follows: N—blue, O—red, Al—turquoise, Ga—silver, C—gray.

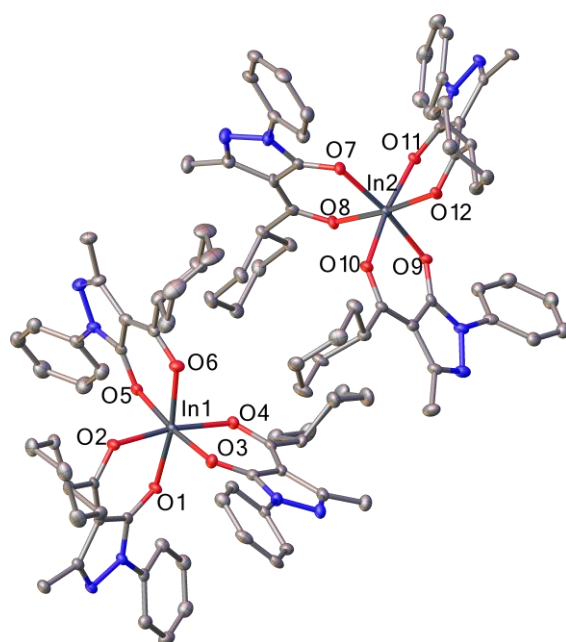


Figure 2. View of the asymmetric unit of $[\text{In}(\text{Q}^{\text{CH}})_3]$. Hydrogen atoms are not shown for clarity. Thermal ellipsoids are illustrated at 50% probability. Central metal atoms and oxygen atoms of ligands are labeled. Atoms are marked by colors as follows: N—blue, O—red, In—silver, C—gray.

2.2.2. Complexes with Rare Earth Elements

Colorless crystals of complexes $[\text{Sc}(\text{Q}^{\text{CH}})_3(\text{DMSO})]$ (6), $[\text{La}(\text{Q}^{\text{CH}})_3(\text{H}_2\text{O})(\text{EtOH})] \cdot (\text{EtOH})$ (7), $[\text{Gd}(\text{Q}^{\text{CH}})_3(\text{H}_2\text{O})]$ (8), and $[\text{Lu}(\text{Q}^{\text{CH}})_3(\text{DMSO})]$ (9), which are suitable for single-crystal X-ray diffraction, were obtained by the slow evaporation of solutions in EtOH for La^{3+} and Gd^{3+} ion complexes or by the slow diffusion of EtOH vapors into a saturated DMSO solutions of complexes for Lu^{3+} and Sc^{3+} ion complexes at room temperature. The selected crystal

data and refinement parameters for complexes $[\text{Sc}(\text{Q}^{\text{CH}})_3(\text{DMSO})]$, $[\text{La}(\text{Q}^{\text{CH}})_3(\text{H}_2\text{O})(\text{EtOH})]\cdot(\text{EtOH})$, $[\text{Gd}(\text{Q}^{\text{CH}})_3(\text{H}_2\text{O})]$, and $[\text{Lu}(\text{Q}^{\text{CH}})_3(\text{DMSO})]$ are listed in Table 2. The isomorphism of the crystal structures of the studied single crystals $[\text{La}(\text{Q}^{\text{CH}})_3(\text{H}_2\text{O})(\text{EtOH})]\cdot(\text{EtOH})$ and $[\text{Gd}(\text{Q}^{\text{CH}})_3(\text{H}_2\text{O})]$ and the corresponding bulk material was confirmed by PXRD (Figures S4 and S6).

Table 2. Crystal data and refinement parameters for $[\text{Sc}(\text{Q}^{\text{CH}})_3(\text{DMSO})]$, $[\text{La}(\text{Q}^{\text{CH}})_3(\text{H}_2\text{O})(\text{EtOH})]\cdot(\text{EtOH})$, $[\text{Gd}(\text{Q}^{\text{CH}})_3(\text{H}_2\text{O})]$, and $[\text{Lu}(\text{Q}^{\text{CH}})_3(\text{DMSO})]$ (6–9).

| Parameter | $[\text{Sc}(\text{Q}^{\text{CH}})_3(\text{DMSO})]$ | $[\text{La}(\text{Q}^{\text{CH}})_3(\text{H}_2\text{O})(\text{EtOH})]\cdot(\text{EtOH})$ | $[\text{Gd}(\text{Q}^{\text{CH}})_3(\text{H}_2\text{O})]$ | $[\text{Lu}(\text{Q}^{\text{CH}})_3(\text{DMSO})]$ |
|--|---|--|---|---|
| Molecular Formula | $\text{C}_{53}\text{H}_{63}\text{ScSn}_6\text{O}_7$ | $\text{C}_{55}\text{H}_{71}\text{LaN}_6\text{O}_9$ | $\text{C}_{51}\text{H}_{59}\text{GdN}_6\text{O}_7$ | $\text{C}_{53}\text{H}_{63}\text{LuSn}_6\text{O}_7$ |
| M | 973.11 | 1099.09 | 1025.29 | 1103.12 |
| Temperature, K | 293(2) | 296(2) | 110(2) | 293(2) |
| System | Triclinic | Monoclinic | Triclinic | Triclinic |
| Space group | P-1 | C2/c | P-1 | P-1 |
| a, Å | 12.8644(8) | 18.4623(13) | 9.8233(8) | 12.9949(13) |
| b, Å | 14.7619(9) | 21.8926(16) | 13.9771(11) | 14.8199(14) |
| c, Å | 15.1365(12) | 27.0312(18) | 18.7740(14) | 15.271(2) |
| α , deg. | 105.270(3) | 90 | 76.367(3) | 105.903(4) |
| β , deg. | 113.938(2) | 103.774(2) | 81.709(4) | 113.978(4) |
| γ , deg. | 90.810(2) | 90 | 77.638(3) | 90.267(3) |
| V, Å ³ | 2510.5(3) | 10,611.5(13) | 2435.0(3) | 2561.7(5) |
| Z | 2 | 8 | 2 | 2 |
| ρ_{calc} , g/cm ³ | 1.287 | 1.376 | 1.398 | 1.430 |
| $\mu(\text{MoK}\alpha)$, mm ⁻¹ | 0.246 | 0.866 | 1.418 | 2.024 |
| F(000) | 1032 | 4576 | 1054 | 1132 |
| $\theta_{\text{min}}-\theta_{\text{max}}$, deg. | 2.40–28.28 | 2.27–26.02 | 1.69–28.00 | 2.10–28.28 |
| Number of measured reflections | 27,067 | 41,943 | 40,875 | 25,256 |
| Number of unique reflections (R_{int}) | 12,396 (0.0951) | 10,447 (0.1536) | 11,740 (0.1026) | 12,647 (0.0283) |
| Number of reflections with $I > 2\sigma(I)$ | 6081 | 6198 | 9736 | 11,216 |
| Number of refined parameters | 618 | 631 | 592 | 618 |
| R-factors ($I > 2\sigma(I)$) | $R_1 = 0.0857$, $\omega R_2 = 0.1572$ | $R_1 = 0.0924$, $\omega R_2 = 0.2088$ | $R_1 = 0.0496$, $\omega R_2 = 0.1040$ | $R_1 = 0.0291$, $\omega R_2 = 0.0550$ |
| R-factors (all reflections) | $R_1 = 0.1775$, $\omega R_2 = 0.1934$ | $R_1 = 0.1543$, $\omega R_2 = 0.2415$ | $R_1 = 0.0640$, $\omega R_2 = 0.1094$ | $R_1 = 0.0365$, $\omega R_2 = 0.0576$ |
| GOOF | 1.000 | 1.018 | 1.026 | 1.020 |
| $\Delta\rho_{\text{max}}/\Delta\rho_{\text{min}}$, e/Å ³ | 0.415/–0.698 | 1.078/–2.214 | 2.177/–1.416 | 0.618/–0.670 |

All four structures are mononuclear complexes, where the metal ion is coordinated by oxygen atoms of three diketonate ligands (Figures 3 and 4) and by oxygen atoms of a number of solvate molecules (one DMSO for $[\text{Sc}(\text{Q}^{\text{CH}})_3(\text{DMSO})]$ and $[\text{Lu}(\text{Q}^{\text{CH}})_3(\text{DMSO})]$, one water and one EtOH for $[\text{La}(\text{Q}^{\text{CH}})_3(\text{H}_2\text{O})(\text{EtOH})]\cdot(\text{EtOH})$, and one water for $[\text{Gd}(\text{Q}^{\text{CH}})_3(\text{H}_2\text{O})]$). It should be noted that $[\text{Sc}(\text{Q}^{\text{CH}})_3(\text{DMSO})]$ and $[\text{Lu}(\text{Q}^{\text{CH}})_3(\text{DMSO})]$ complexes are isostructural.

It should also be noted that, according to the PXRD data (Figure S5), the $[\text{Sc}(\text{Q}^{\text{CH}})_3(\text{H}_2\text{O})]$ and $[\text{Lu}(\text{Q}^{\text{CH}})_3(\text{H}_2\text{O})]$ complexes also turned out to be isostructural; however, due to the depressingly low solubility levels in most of the weak or moderate coordinating solvents, it was not possible to grow the single crystals of these compounds.

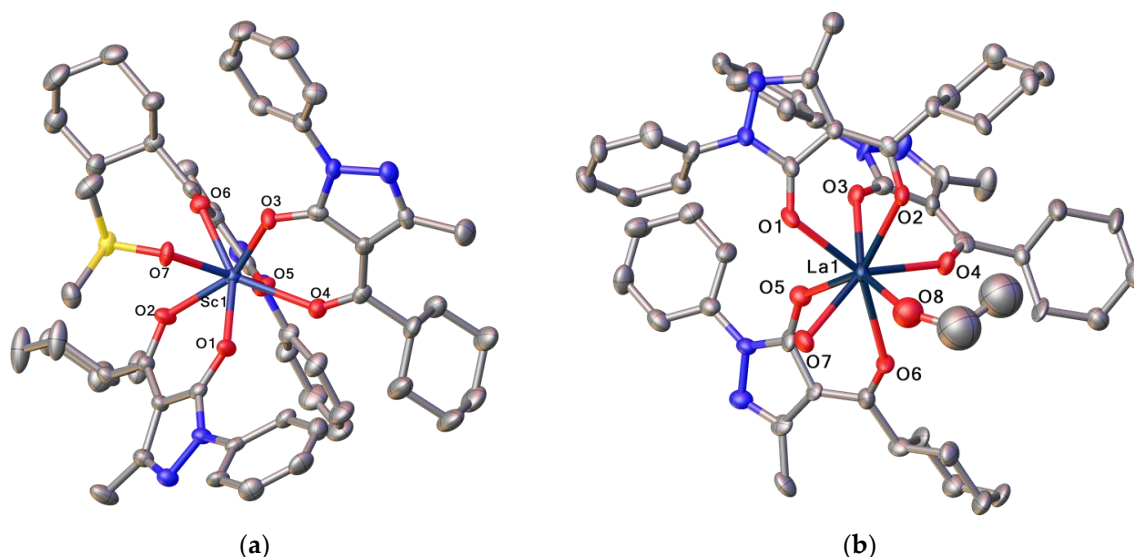


Figure 3. View of the asymmetric unit of $[\text{Sc}(\text{Q}^{\text{CH}})_3(\text{DMSO})]$ (a) and $[\text{La}(\text{Q}^{\text{CH}})_3(\text{H}_2\text{O})(\text{EtOH})]\cdot(\text{EtOH})$ (b). Hydrogen atoms and solvated EtOH molecule in (b) are not shown for clarity. Thermal ellipsoids are illustrated at 50% probability. Central metal atoms and oxygen atoms of ligands are labeled. Atoms are marked by colors as follows: N—blue, O—red, Sc—silver-blue, La—dark blue, S—yellow, C—gray.

At the same time, the slow diffusion of EtOH vapors into the solutions of hydrated complexes in DMSO led to the other crystal structures, namely $[\text{Sc}(\text{Q}^{\text{CH}})_3(\text{DMSO})]$ (6) or $[\text{Lu}(\text{Q}^{\text{CH}})_3(\text{DMSO})]$ (9), having one coordinated DMSO molecule instead of a water molecule. This alteration does not affect the coordination polyhedron $\{\text{MO}_7\}$, which is a capped trigonal prism in all cases, but rather leads to a slight change in the relative arrangement of the ligands around the metal ion (Figure S7).

As for the $[\text{La}(\text{Q}^{\text{CH}})_3(\text{H}_2\text{O})(\text{EtOH})]\cdot(\text{EtOH})$ (7) complex, a relatively larger ionic radius of La^{3+} compared to Sc^{3+} , Gd^{3+} , and Lu^{3+} ions causes the formation of an octa-coordinated complex that includes two solvent molecules in the inner coordination sphere, leading to the $\{\text{MO}_8\}$ La^{3+} polyhedron, which is best described as a square antiprism.

The analysis of Ln^{3+} -O bond lengths in the corresponding La^{3+} , Gd^{3+} , and Lu^{3+} ion complexes (Table S2) allows one to observe the influence of lanthanide contraction, which results not only in the shortening of bond lengths, but also in changes in the coordination number from eight for $[\text{La}(\text{Q}^{\text{CH}})_3(\text{H}_2\text{O})(\text{EtOH})]\cdot(\text{EtOH})$ to seven for $[\text{Gd}(\text{Q}^{\text{CH}})_3(\text{H}_2\text{O})]$ and $[\text{Lu}(\text{Q}^{\text{CH}})_3(\text{DMSO})]$. It is also worth noting that the hepta-coordinated lanthanide ion is observed in Eu^{3+} [29] and Dy^{3+} [42] complexes that are isostructural to $[\text{Gd}(\text{Q}^{\text{CH}})_3(\text{H}_2\text{O})]$.

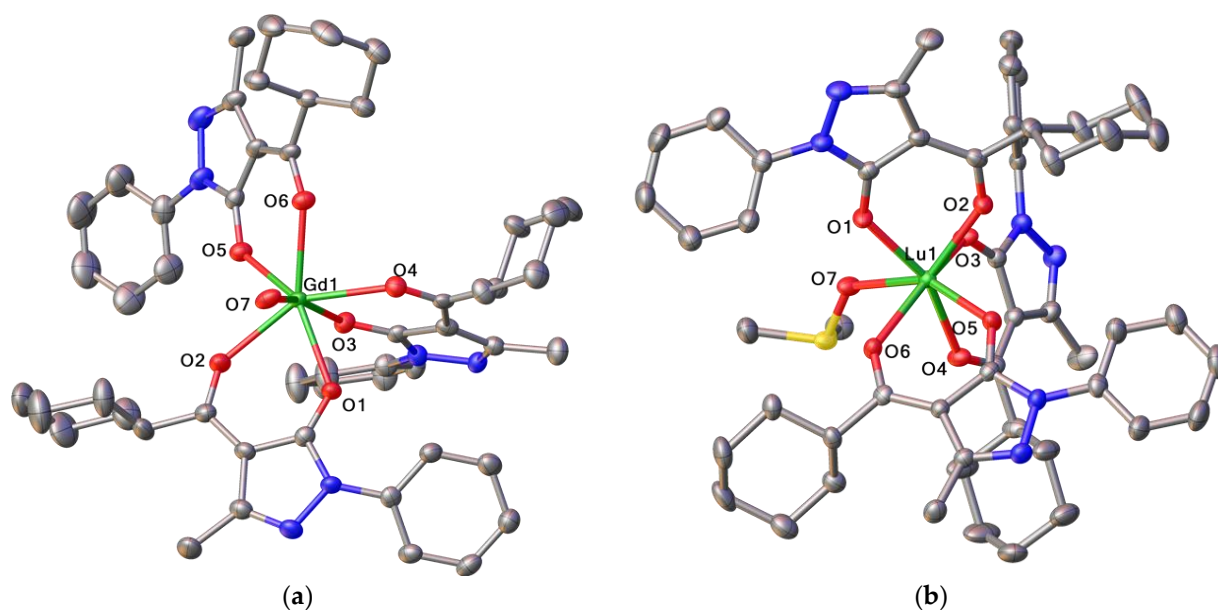


Figure 4. View of the asymmetric unit of $[\text{Gd}(\text{Q}^{\text{CH}})_3(\text{H}_2\text{O})]$ (a) and $[\text{Lu}(\text{Q}^{\text{CH}})_3(\text{DMSO})]$ (b). Hydrogen atoms are not shown for clarity. Thermal ellipsoids are illustrated at 50% probability. Central metal atoms and oxygen atoms of ligands are labeled. Atoms are marked by colors as follows: N—blue, O—red, Gd or Lu—green, S—yellow, C—gray.

The analysis of the crystal packing of isostructural $[\text{Sc}(\text{Q}^{\text{CH}})_3(\text{DMSO})]$ and $[\text{Lu}(\text{Q}^{\text{CH}})_3(\text{DMSO})]$ complexes did not reveal any strong intermolecular hydrogen bonds besides rather weak $\text{CH} \dots \pi$ interactions. On the contrary, the crystal packing of $[\text{Gd}(\text{Q}^{\text{CH}})_3(\text{H}_2\text{O})]$ additionally contains a number of $\text{O}-\text{H} \dots \text{N}$ hydrogen bonds (the $\text{O}7 \dots \text{N}2$ distance is 2.776 Å; the $\text{O}7 \dots \text{N}4$ distance is 2.703 Å, see Figure S8). As for $[\text{La}(\text{Q}^{\text{CH}})_3(\text{H}_2\text{O})(\text{EtOH})] \cdot (\text{EtOH})$, a solvated EtOH molecule assists in the formation of a large amount of $\text{O}-\text{H} \dots \text{O}$ and $\text{O}-\text{H} \dots \text{N}$ intermolecular interactions (the $\text{O}7 \dots \text{N}6$ distance is 2.791 Å; the $\text{O}8 \dots \text{O}9$ distance is 2.934 Å; the $\text{O}9 \dots \text{N}2$ distance is 2.720 Å, see Figure S9)

2.3. Spectroscopic Studies

Optical absorption spectra were obtained for all the complexes and HQ^{CH} (1). As can be seen in Figure 5, the absorption spectra exhibit two pronounced absorption bands located in the UV region of spectra. The bands correspond to ligand absorption and we observed no ion absorption for any of the complexes. The spectra recorded for the complexes $[\text{La}(\text{Q}^{\text{CH}})_3(\text{H}_2\text{O})(\text{EtOH})]$, $[\text{Lu}(\text{Q}^{\text{CH}})_3(\text{H}_2\text{O})]$, and $[\text{Gd}(\text{Q}^{\text{CH}})_3(\text{H}_2\text{O})]$, designated further as **La**, **Lu**, and **Gd**, respectively, qualitatively resemble the spectrum of HQ^{CH} . However, the molar extinction (ϵ) increases from 6×10^3 for HQ^{CH} to $3.2\text{--}5.5 \times 10^4 \text{ L} \times \text{mol}^{-1} \times \text{cm}^{-1}$ for complexes. Moreover, ϵ increases monotonically from 2.2×10^4 to $5.5 \times 10^4 \text{ L} \times \text{mol}^{-1} \times \text{cm}^{-1}$ with the replacement of the central ion by one with a higher atomic number. On the contrary, the 13 group metal and Sc^{3+} ions affect the optical absorption of the complexes $[\text{Sc}(\text{Q}^{\text{CH}})_3(\text{H}_2\text{O})]$ and $[\text{M}(\text{Q}^{\text{CH}})_3]$, $\text{M} = \text{Al}, \text{In},$ and Ga (designated as **Sc**, **Al**, **In**, and **Ga**, respectively), by two factors. Firstly, they multiply ligand extinction up to 10 times. Secondly, these complexes have the red-shift of absorption bands in comparison with the complexes of lanthanide ions and HQ^{CH} . The maximum red-shift of an absorption band is observed for the **Sc** complex. Notably, the absorption bands are better resolved in the spectra recorded for the **Al**, **Sc**, **In**, and **Ga** complexes than that in the spectra recorded for HQ^{CH} and lanthanide ion complexes. This is caused by the redistribution of the oscillator strengths corresponding to these bands [15].

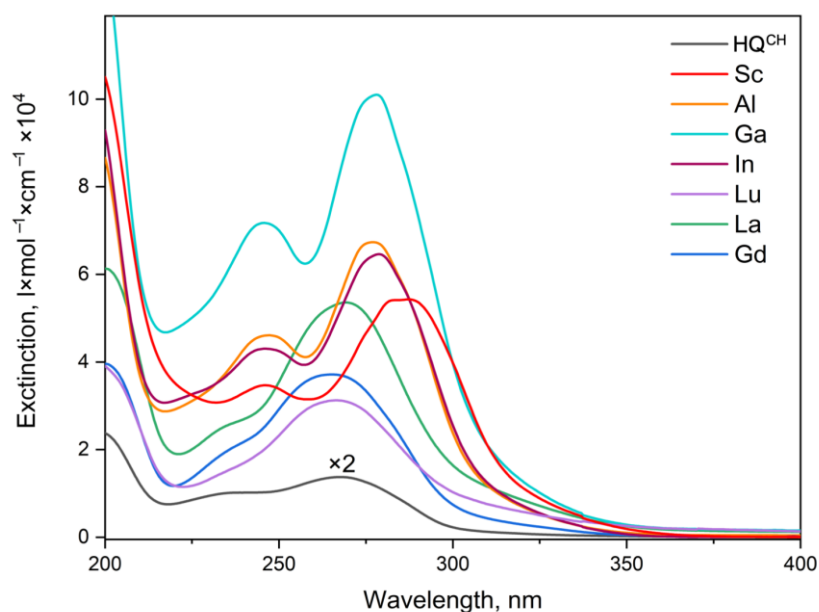


Figure 5. UV-Vis spectra for the compounds in acetonitrile (MeCN).

Photoluminescence (PL) spectra, measured under excitations at 340 nm wavelengths, are shown on Figure 6. The spectrum of $H \rightarrow Q^{CH}$ reveals a wide spectral band (FWHM = 92 nm) with the emission maximum at 530 nm and with a wide shoulder at longer wavelengths up to 800 nm. Additionally, the additional fluorescence band appears within the region of 380–420 nm. We observed significant influences of the central ion on the PL spectrum. Actually, the emission maximum (λ_{em}) shifts to the blue region of the optical spectrum from 530 nm for the HQ^{CH} ligand to 490 nm for **Gd**, 464 nm for **In** and **Ga**, and 458 nm for **Al**. Finally, the maximum blue-shift of the PL maximum is for **Sc**, **La**, and **Lu**, measuring 430, 436, and 428 nm, respectively. Surprisingly, the spectrum taken for **Gd** exhibits a wide spectral band (FWHM = 104 nm) and the maximum is centered at 490 nm. There is a low intensity spectral band located within 380–420 nm, which matches with the PL maxima of the **Sc**, **La**, and **Lu** complexes. We suppose that the redistribution of the emission intensity is determined by the presence of dual emission: ligand phosphorescence located at longer wavelengths and ligand fluorescence at 425 nm.

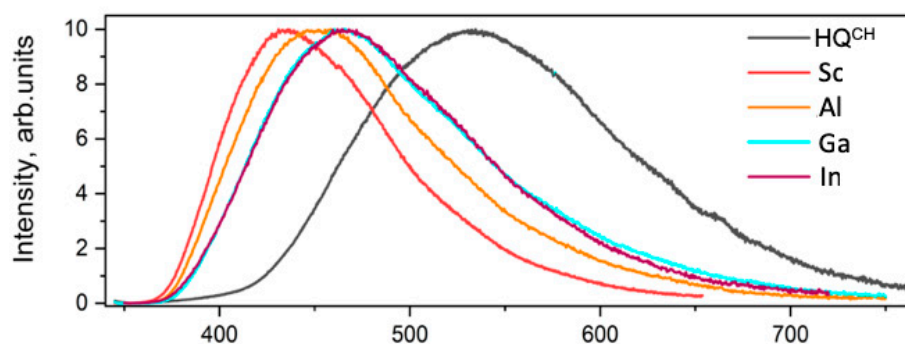


Figure 6. Cont.

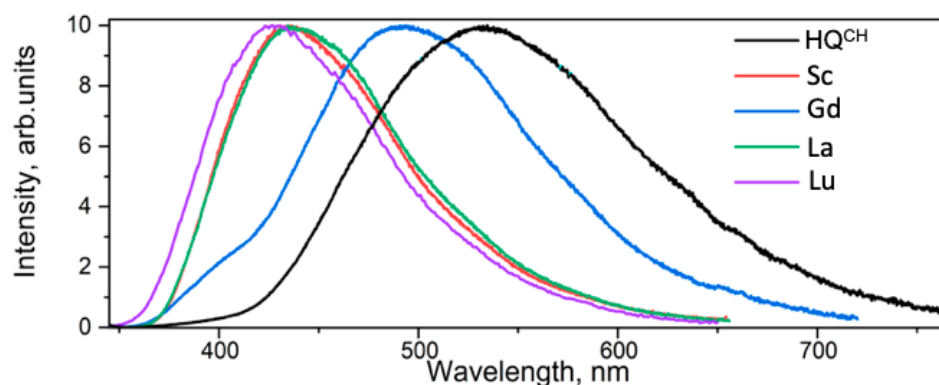


Figure 6. Photoluminescence spectra for the compounds in solid state under CW excitation at 340 nm.

To check this hypothesis, the fluorescence and phosphorescence spectra at 77 K were measured (see Figure 7). It is clearly noticeable that the spectral band in the short-wave region of the phosphorescence spectrum disappears, while in the spectrum without delay (fluorescence spectrum), the band is still observed, which unequivocally confirms the fluorescent nature of this spectral band.

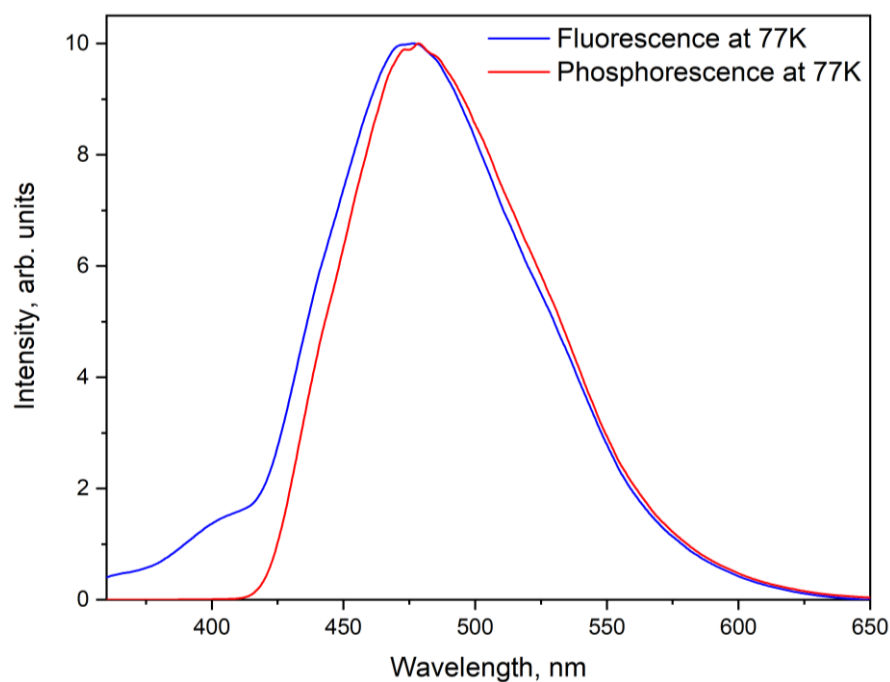


Figure 7. Photoluminescence spectra of $[\text{Gd}(\text{Q}^{\text{CH}})_3(\text{H}_2\text{O})]$ (**8**) at temperature 77 K.

A comparison between the spectra recorded for the complexes of lanthanide ions and those for the complexes of the 13 group metals implies that the valence electrons caused the shift of the emission maximum toward 458 nm for **Al** and 464 nm for **In**.

Photoluminescence excitation (PL) spectra were obtained for all the compounds and HQ^{CH} with the registration wavelength located at the emission maxima, respectively. All the spectra are qualitatively similar, revealing a broad excitation band at 320–400 nm. An excitation maximum of 361 nm was estimated for the free ligand (HQ^{CH}) under emission registration at 530 nm, whereas the spectra for complexes revealed a blue-shifted excitation band with the maxima located in a neighborhood of 340 nm, except for the **Lu** complex (see Figure 8 and Table 3).

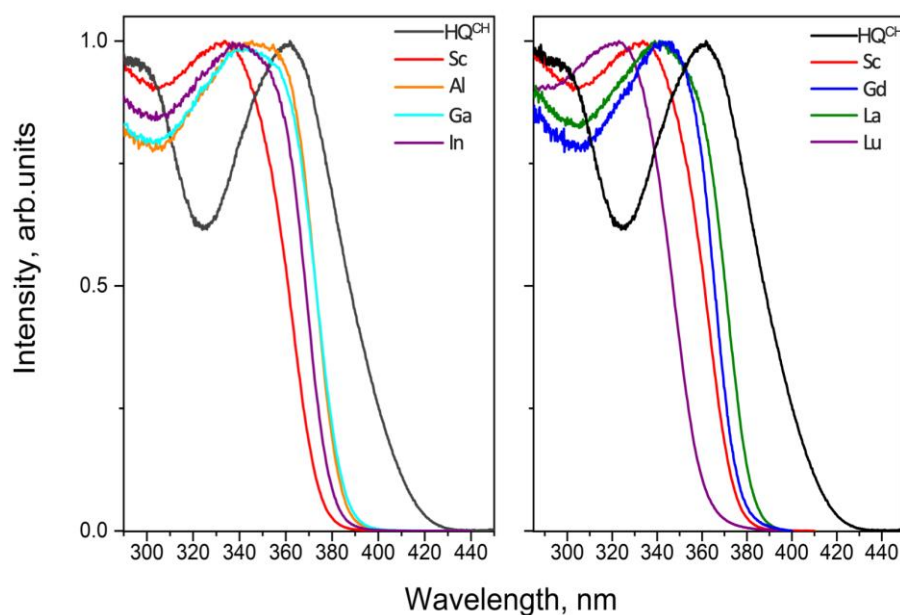


Figure 8. PL excitation spectra for compounds at solid state with registration wavelengths at PL maxima.

Table 3. Photophysical parameters for all the compounds.

| Compound | λ_{abs} nm | λ_{em} nm | λ_{exc} nm | $E(S_1) \times 10^3$ cm^{-1} | $E(T_1) \times 10^3$ cm^{-1} | Energy Gap $\times 10^3$ cm^{-1} | τ_{obs} ns | Φ % |
|------------------|------------------------------|-----------------------------|------------------------------|--|--|--|--|----------------|
| HQ ^{CH} | 267 | 530 | 361 | 26.0 | 22.1 | 3.9 | 7.4 ± 0.1 | 0.5 ± 0.1 |
| Sc | 271 | 430 | 338 | 27.3 | 22.7 | 4.5 | 2.7 ± 0.1 6.3 ± 0.1 | 10.6 ± 0.1 |
| La | 269 | 436 | 339 | 27.4 | 23.6 | 3.8 | 3.4 ± 0.1 8.7 ± 0.1 | 19.5 ± 0.1 |
| Gd | 265 | 490 | 343 | 27.7 | 23.6 | 4.1 | $(22.3 \pm 0.2) \times 10^3$ $(36.5 \pm 0.3) \times 10^3$ | 19.0 ± 0.1 |
| Lu | 276 | 428 | 323 | 28.0 | 23.7 | 4.3 | 1.7 ± 0.1 4.1 ± 0.1 | 6.5 ± 0.1 |
| Al | 277 | 458 | 345 | 27.6 | 23.7 | 3.8 | 9.8 ± 0.1 | 16.9 ± 0.1 |
| Ga | 278 | 463 | 342 | 27.0 | 23.5 | 3.5 | 6.3 ± 0.1 | 6.6 ± 0.1 |
| In | 278 | 464 | 340 | 27.6 | 23.6 | 4.0 | 4.2 ± 0.1 | 3.0 ± 0.1 |

To gain insight into the electronic excitation relaxation processes in the investigated compounds, luminescence decays were recorded. All the experiments were conducted at room temperature. As seen from Table 3 (see Figure S10), the formation of trivalent ion complexes increases the observable luminescence lifetime (τ) in comparison with HQ^{CH}. The luminescence decays recorded for the *p*-metal ion complexes Al, Ga, and In reveal single exponential behavior with characteristic lifetimes of $\tau = 9.9$, 6.3, and 4.2 ns, respectively. Therefore, the replacement of the central Al³⁺ ion with the heavier one (Ga³⁺ and In³⁺) leads to a decrease in the observed lifetimes of up to two times. On the contrary, the decays obtained for rare earth ion complexes have more complicated behaviors. The multiexponential law can fit the recorded kinetic traces:

$$I_{\text{th}}(t) = \sum_{i=1}^n A_i e^{-\frac{t}{\tau_i}} \quad (1)$$

where τ_i and A_i are decay times and amplitudes, respectively. The measured luminescence decay is determined by the following equation:

$$I_{\text{exp}}(t) = \int_0^{\infty} I_{\text{irf}}(t') I_{\text{th}}(t - t') dt' \quad (2)$$

where $I_{\text{irf}}(t')$ is the instrument response function (IRF), which can be described as a double Gaussian shape with the characteristic lifetime of $\tau_{\text{irf}} = 0.5$ ns.

Specifically, the decays for the complexes of the La^{3+} , Lu^{3+} , and Sc^{3+} ions fit with the bi-exponential function. The presence of two relaxation components in the fluorescence decays of the Sc, La, and Lu complexes can be attributed to the distinct emitting sites that are responsible for luminescence [15]. Their characteristic lifetimes are listed in Table 3. Unexpectedly, the luminescence of the **Gd** compound has a significantly longer decay with characteristic lifetimes of $\tau_1 = 22$ μs and $\tau_2 = 36$ μs (see Figure S11). Therefore, the relatively long lifetime proves the phosphorescence nature of long wavelength bands in the PL spectrum for **Gd**. We also measured the luminescence decay for the **Gd** compound at a cryogenic temperature of 77 K. Cooling leads to the suppression of all the rotational–vibrational processes with consequentially higher values of characteristic lifetimes of $\tau^{77}_1 = 220$ μs and $\tau^{77}_2 = 536$ μs .

3. Discussion

The energies of the first excited singlet and triplet states were estimated by generally recognized methods [25,53]. Due to the energy reorganization in absorption and emission processes for the non-adiabatic approximation, energies of the $S_0 \rightarrow S_1$ and $T_1 \rightarrow S_0$ transitions can be determined as the low-energy edges of the absorption spectrum and high-energy edges of the phosphorescence spectrum with the use of the tangent method [25]. To suppress the rotational–vibrational processes during phosphorescence measurements, the complexes were cooled down to 77 K. To remove the fast fluorescence contribution, a 200 μs delay was employed. The estimated energies of the T_1 state are listed in Table 3. We obtained the close values for all the complexes, which lie in the range of 23,500–23,700 cm^{-1} , except for Sc. An energy of 22,715 cm^{-1} was obtained for Sc. Therefore, the central ion leads to a T_1 state energy increase from 22,100 cm^{-1} for **HQ^{CH}** to 22,715 cm^{-1} for **Sc** and approximately 23,600 cm^{-1} for all other complexes.

The first excited singlet state energy (S_1) increases for all the complexes in comparison with **HQ^{CH}**, which has an S_1 energy of 26,000 cm^{-1} . The highest energy was obtained for Lu—28,000 cm^{-1} ; other complexes' energies lay in the range of 27,000–27,700 cm^{-1} . Thereby, we did not observe significant changes in the energy gap (ΔE_{ST}) between the S_1 and T_1 states due to the influence of ion substitution (see Table 3).

It should be noted that the ΔE_{ST} values of the **La** and **Gd** complexes are sufficiently close to the ligand's values. As ΔE_{ST} values of **La** and **Gd** and the ligand are close, and the **La** and **Gd** absorption spectra qualitatively resemble the ligand's one, we consider that, specifically, La^{3+} and Gd^{3+} do not distort the potential energy surfaces of the S_1 and T_1 states.

Figure 7 demonstrates the fluorescence and phosphorescence spectra obtained for the **Gd** complex. The emission spectrum, recorded at 77 K, reveals two emission bands located at 380–420 nm and at 420–650 nm. The band located in the region 380–420 nm vanishes in the phosphorescence spectrum, proving the presence of two radiative relaxation processes with different emission states for the **Gd** complex. Namely, fluorescence appears within 380–420 nm and phosphorescence is observed on a long-wavelength spectral range. It is interesting that, according to the literature, room temperature phosphorescence is quite rare to see [7,54,55].

Therefore, there are two possible explanations for this phenomenon. First, the inter-system crossing process (ISC) of the **Gd** complex has a higher rate compared with the other complexes. The second explanation is that it has a much lower rate of non-radiative processes due to the different molecule structures and different symmetry groups in particular.

Two observed lifetimes can be assigned to radiative relaxation from two local minima on the T_1 state's potential energy surface (PES). Since the long time component's lifetime is much higher under cooling than the short time component's lifetime, we conclude that the longest time component (τ_2) is associated with radiative relaxation from the deepest minimum of T_1 PES. For all the investigated complexes, we measured the PL quantum yield values Φ under optical excitations at 340 nm, providing excitations in the maximum of the luminescence excitation spectra (see Figure 4). As follows from Table 3, the formation of complexes leads to strong increases in the PL quantum yield by up to 39 times. In particular, the maximum Φ value was recorded for **La**. In this compound ligand, the fluorescence Φ was enhanced from 0.5% to 19.5%. In the 13 group metal complexes, the replacement of the central ion with a heavier one led to a decrease in the quantum yield value from 16.9% for **Al** to 6.6% for **Ga** and 3.3% for **In**. We see the same dependence for the **La** (19.5%) and **Lu** (6.5%) complexes. The probabilities of radiative (k_{rad}) and non-radiative (k_{nrad}) processes were evaluated using the following formulas [53]:

$$k_{\text{rad}} = \frac{\Phi}{\tau_{\text{obs}}} \quad (3)$$

$$\tau_{\text{obs}} = \frac{1}{k_{\text{rad}} + k_{\text{nrad}}} \quad (4)$$

$$k_{\text{nrad}} = \frac{1}{\tau_{\text{obs}}} - k_{\text{rad}} \quad (5)$$

As can be seen from Tables 3 and 4, the rate of the radiative process monotonically reduces from 1.7×10^7 to $0.7 \times 10^7 \text{ s}^{-1}$, and the quantum yield decreases from 16.9 to 3.0 under the replacement of the central Al^{3+} ion on Ga^{3+} and In^{3+} . Notably, the fluorescence quantum yield value recorded for the **Gd** complex is only 1.8%, since the radiative relaxation of S_1 is a less pronounced pathway than the intersystem crossing process (ISC) followed by phosphorescence. As we noted a significant increase in the observed luminescence lifetime under cooling up to 77 K, a huge enhancement of the quantum yield was expected. While the number of emitted photons equals the integrated intensity of the emission spectrum, the luminescence quantum yield at a temperature of 77 K (Φ_{77}) can be calculated by the following formula:

$$\Phi_{77} = \frac{I_{77}}{I_{300}} \Phi_{300} \quad (6)$$

where I_{77} integrated luminescence intensity at 77 K, I_{300} integrated luminescence intensity at 300 K, and Φ_{300} quantum yield at 300 K. According to this procedure, we achieved the quantum yield value of 45.8% for the **Gd** complex at a temperature of 77 K.

Table 4. Radiative (k_{rad}) and non-radiative (k_{nrad} , k_{isc}) rate constants in s^{-1} for the **Al**, **In**, **Ga**, and **Gd** compounds (2-4 and 8) and free ligand (1).

| Compound | $k_{\text{rad}} \times 10^7$ | $k_{\text{nrad}} \times 10^8$ | ^a $k_{\text{isc}} \times 10^7$ | ^b $k_{\text{isc}} \times 10^7$ |
|------------------|------------------------------|-------------------------------|---|---|
| HQ ^{CH} | 0.1 | 1.4 | 13.4 | 13.3 |
| Al | 1.7 | 1.0 | 8.5 | 6.3 |
| Ga | 1.0 | 1.6 | 14.8 | 8.6 |
| In | 0.7 | 2.4 | 23.3 | 8.9 |
| Gd | - | - | 12.5 | 13.8 |

^a Measured at 300 K, ^b measured at 77 K.

To estimate the energy transfer process from a singlet state to a triplet manifold, the intersystem crossing rates (k_{isc}) were calculated using emission lifetimes and fluorescence quantum yields, both at 300 K and 77 K. Since only the **Al**, **In**, **Ga**, and **Gd** complexes and HQ^{CH} demonstrate the single exponential fluorescence behavior, calculations were

only performed for these compounds. The intersystem crossing rate can be evaluated as follows [25]:

$$k_{\text{isc}} = \frac{1 - \Phi}{\tau_{\text{obs}}}. \quad (7)$$

After comparing the ISC rates obtained at 300 K and 77 K, we conclude that the rates for the **Al**, **In**, and **Ga** complexes are lower at 77 K. This is caused by significant vibrational relaxation at room temperature. Taking into account the fact that the probability of non-radiative vibrational relaxation processes is negligibly low at 77 K, we assume that the applied method is more beneficial for calculations at 77 K. The rates calculated at 77 K increase with an increase in the atomic number of the 13 group ions. The k_{isc} rate of the **HQ^{CH}** rate remained unchanged with the decrease in the temperature ($13.4 \times 10^7 \text{ s}^{-1}$ and $13.3 \times 10^7 \text{ s}^{-1}$ at 300 K and 77 K, respectively), suggesting that phosphorescence is predominant in the relaxation channel (see Figure 6). On the contrary, the **Gd** complex rate slightly increases from $12.5 \times 10^7 \text{ s}^{-1}$ (300 K) to $13.8 \times 10^7 \text{ s}^{-1}$ (77 K) due to the paramagnetic properties of the Gd^{3+} ion (See Table 4). Notably, since the **Gd** compound has a rigid geometry, vibrational relaxation is reduced in comparison with **HQ^{CH}**. Therefore, phosphorescence in the **Gd** complex is more effective relaxation pathway (see Table 3).

4. Materials and Methods

Common reagents were purchased from Aldrich (St. Louis, MO, USA) and were used without further purification. Ligand-1-phenyl-3-methyl-4-cyclohexylcarbonyl-pyrazol-5-one (**HQ^{CH}**, **1**) was synthesized according to previously published procedure [42]. Rare earth compounds of high purity (99.99–99.999%) were purchased from Lanhit (Moscow, Russia).

Stock 1 M $\text{Sc}(\text{ClO}_4)_3$ solution was prepared as follows: after being freshly calcinated at 600 °C, Sc_2O_3 (6.896 g, 50 mmol, 99.999%) was dissolved upon heating in a quartz flask in mixture of 26 mL of perchloric acid (70%, 99.999% trace metals basis, Aldrich) and 20 mL of deionized water. Excess water was slowly evaporated at 90 °C; the residue was quantitatively transferred to a 100 mL volumetric flask and brought to volume by deionized water. Solution was stored in a polypropylene bottle.

Elemental analysis was performed by Elemental Vario MicroCube CHNO(S) analyzer (Elementar Analysensysteme, Langenselbold, Germany). The metal content was determined by complexometric titration with a Trilon B (disodium salt of ethylenediaminetetraacetic acid) solution in the presence of Xylenol Orange as an indicator (for scandium, lanthanum, and lutetium) or by ICP-MS analysis (for aluminum, gallium, and indium). Before the analysis, the complexes were decomposed by heating with concentrated HNO_3 . ICP-MS was performed using an inductively coupled plasma mass spectrometer ELAN mod. 9000, DRC II, DRC-e (PerkinElmer, Waltham, MA, USA). FTIR spectra were recorded in KBr pellets on Perkin Elmer Spectrum One instrument (PerkinElmer, Waltham, MA, USA).

Single-crystal X-ray diffraction analysis of $[\text{Al}(\text{Q}^{\text{CH}})_3]$, $[\text{Ga}(\text{Q}^{\text{CH}})_3]$, $[\text{In}(\text{Q}^{\text{CH}})_3]$, $[\text{Sc}(\text{Q}^{\text{CH}})_3(\text{DMSO})]$, $[\text{La}(\text{Q}^{\text{CH}})_3(\text{H}_2\text{O})(\text{EtOH}) \cdot (\text{EtOH})]$, $[\text{Gd}(\text{Q}^{\text{CH}})_3(\text{H}_2\text{O})]$, and $[\text{Lu}(\text{Q}^{\text{CH}})_3(\text{DMSO})]$ was carried out on a Bruker D8 Quest (Bruker, Billerica, MA, USA) diffractometer (MoK α radiation, ω and φ -scan mode). The structures were solved with direct methods and refined by least-squares method in the full-matrix anisotropic approximation on F^2 . High reported values of R_1 -factors for $[\text{Al}(\text{Q}^{\text{CH}})_3]$ and $[\text{Ga}(\text{Q}^{\text{CH}})_3]$ were due to their weak scattering of X-ray caused by disorders of cyclohexyl substituents. All hydrogen atoms were located in calculated positions and refined within riding model. All calculations were performed using the SHELXTL [56,57] and Olex2 [58] software packages. Atomic coordinates, bond lengths, angles, and thermal parameters have been deposited at the Cambridge Crystallographic Data Centre with deposition numbers—CCDC 2208569–2208571, 2215463, 2215494, 2215723, and 2215486, which are all available, free of charge at www.ccdc.cam.ac.uk (accessed on 3 April 2023).

Powder X-ray diffraction (PXRD) patterns were measured on D/MAX 2500 (Rigaku Corporation, Tokyo, Japan) diffractometer in the reflection mode with $\text{CuK}\alpha_1$ radiation ($\lambda = 1.54056 \text{ \AA}$) and curved graphite [002] monochromator placed in the reflected beam.

Optical absorption spectra of Ln^{3+} compounds and HL dissolved in acetonitrile (HPLC SuperGradient, Panreac, Spain) were recorded using JASCO V-770 (Jasco, Tokyo, Japan) spectrophotometer operating within 200–2500 nm. Concentrations of the solutions were approximately 10^{-5} M/L . For solutions, the measurements were performed using quartz cells with a 1 cm pathlength. Photoluminescence spectra and luminescence excitation spectra were measured using Horiba Jobin-Yvon Fluorolog QM-75-22-C spectrofluorimeter using a 75 W xenon arc lamp (PowerArc, HORIBA, Kyoto, Japan). A Hamamatsu R13456 (Hamamatsu Photonics, Hamamatsu, Japan) cooled photomultiplier tube sensitive in UV–Vis–NIR region (200–950 nm) was used as the detector. Photoluminescence quantum yields were obtained for solid samples by absolute method with the use of same experimental setup, which were equipped with integration sphere G8 (GMP, Renens, Switzerland). Photoluminescence decays were measured by time-correlated single photon counting (TCSPC) method using the same spectrofluorimeter. The setup included DeltaLED (HORIBA, Kyoto, Japan) as a pulsed excitation source emitting at 340 nm with a repetition rate of 6.25 MHz and pulse duration FWHM of 0.6 ns. For all optical measurements, the corresponding instrument response functions were taken into account. The experiments were performed in air at atmospheric pressure. Degradation of the optical properties was not observed during the experiments.

IR spectra were registered in the range $4000\text{--}400 \text{ cm}^{-1}$ in KBr pellets using a Perkin-Elmer system Spectrum One 100 FTIR (PerkinElmer, Waltham, MA, USA) spectrometer. IR spectra of all complexes are given in Figure S12.

Nuclear magnetic resonance (NMR) spectra were recorded in $(\text{CD}_3)_2\text{CO}$ or $\text{DMSO-}d_6$ solutions at 298 K on a Bruker AC-300 (Bruker, Billerica, MA, USA) spectrometer operating at 300.13 MHz for ^1H . TMS ($\delta = 0.00 \text{ ppm}$), which was used as a standard.

Synthesis of $[\text{Al}(\text{Q}^{\text{CH}})_3]$ (2), $[\text{In}(\text{Q}^{\text{CH}})_3]$ (3) and $[\text{Ga}(\text{Q}^{\text{CH}})_3]$ (4)

Ligand HQ^{CH} (1) (0.426 g, 1.5 mmol) was dissolved in 10 mL of EtOH (96%) at $45 \text{ }^\circ\text{C}$ and 0.5 mmol solution of corresponding hydrated chloride or nitrate (0.121 g of $\text{AlCl}_3 \cdot 6\text{H}_2\text{O}$, 0.209 g of $\text{Ga}(\text{NO}_3)_3 \cdot 9\text{H}_2\text{O}$, or 0.147 g $\text{InCl}_3 \cdot 4\text{H}_2\text{O}$) in 2 mL of boiling EtOH, was added slowly with continuous magnetic stirring. The mixture was stirred for 5 min at $45 \text{ }^\circ\text{C}$, and then 1.5 mL (1.5 mmol) of 1 M NaOH solution in EtOH was added dropwise. The resulting solution was stirred in a closed vial for additional 4 h at $45 \text{ }^\circ\text{C}$, cooled to room temperature, and precipitate was separated. The precipitate was washed successively with 8 mL of 20% aqueous EtOH, 8 mL of deionized water, and 5 mL of hexane, and dried at $40 \text{ }^\circ\text{C}$ and 0.1 torr to a constant weight.

Tris-(4-(cyclohexylcarbonyl)-5-methyl-2-phenyl-2,4-dihydro-3H-pyrazol-3-onato) aluminum (III), $[\text{Al}(\text{Q}^{\text{CH}})_3]$ (2)

Slightly pink powder: yield is 0.364 g (83%). Anal. calcd. for $\text{C}_{51}\text{H}_{57}\text{AlN}_6\text{O}_6$ (877.02): C, 69.84; H, 6.55; N, 9.58; Al, 3.08; found: C, 69.89; H, 6.61; N, 9.65; Al, 3.11%. IR: 3061 w; 2929 m ν_{as} CH (cyclohexyl); 2855 m ν_{s} CH (cyclohexyl); 2664 w; 2532 w; 2353 w; 1943 w; 1869 w; 1793 w; 1612 vs. $\nu(\text{C}=\text{O})$; 1596 s $\nu(\text{C}=\text{C}, \text{C}=\text{N})$; 1584 s; 1537 s; 1519 s; 1498 vs. $\nu(\text{C}=\text{C}, \text{C}=\text{N})$; 1465 s; 1442 s; 1415 m; 1391 s; 1364 w; 1351 w; 1246 w; 1178 w; 1158 w; 1141 w; 1126 w; 1083 s; 1066 m; 1027 m; 1010 w; 1001 w; 985 m δ_{r} (C-H cyclohexyl); 924 w; 907 w; 894 w; 873 w; 845 w; 821 m; 792 w; 771 w; 758 m; 725 w; 690 m; 660 m; 642 w; 632 w; 615 vw; 549 w; 524 w; 510 w; 497 w; 448 vw; 415 w; 407 w. $^1\text{H-NMR}$ (acetone- d_6): 8.08–7.72 (m, 2H, o- C_6H_5); 7.38 (t, 1.08H, p- C_6H_5); 7.28–7.08 (m, 1.95H, m- C_6H_5); 3.08 (m, 1.01H, HC-C=O); 2.47 (m, 3.16H, CH_3), 1.89–1.09 (m, 10.33H, cyclohexyl).

Tris-(4-(cyclohexylcarbonyl)-5-methyl-2-phenyl-2,4-dihydro-3H-pyrazol-3-onato) indium (III), $[\text{In}(\text{Q}^{\text{CH}})_3]$ (3)

Slightly yellow powder: yield is 0.354 g (77%). Anal. calcd. for $\text{C}_{51}\text{H}_{57}\text{InN}_6\text{O}_6$ (964.85): C, 63.49; H, 5.95; N, 8.71; In, 11.90; found: C, 63.44; H, 6.12; N, 8.90; In, 12.08%. IR: 3047 m; 2931 m ν_{as} CH (cyclohexyl); 2855 m ν_{s} CH (cyclohexyl); 2665 w; 2354 w; 2250 w; 1944 w;

1885 w; 1794 w; 1737 w; 1603 s $\nu(\text{C}=\text{O})$; 1592 s $\nu(\text{C}=\text{C}, \text{C}=\text{N})$; 1574 vs; 1535 s; 1485 vs. $\nu(\text{C}=\text{C}, \text{C}=\text{N})$; 1461 s; 1441 m; 1405 m; 1382 s; 1362 m; 1350 w; 1323 w; 1238 w; 1178 w; 1140 w; 1077 m; 1066 m; 1027 w; 1011 w; 1001 w; 982 m $\delta_r(\text{C}-\text{H}$ cyclohexyl); 922 w; 908 w; 893 w; 870 w; 842 w; 815 w; 791 w; 767 w; 757 m; 711 w; 690 w; 668 vw; 656 w; 644 vw; 622 w; 614 w; 511 w; 503 w; 466 w; 446 vw; 419 vw; 412 vw; 404 vw. $^1\text{H-NMR}$ (acetone- d_6): 7.89–7.85 (m, 2H, o- C_6H_5); 7.37–7.32 (m, 2.00H, m- C_6H_5); 7.22–7.19 (m, 1.04H, p- C_6H_5); 3.12 (m, 1.01H, HC-C=O); 2.45 (m, 3.07H, CH_3), 1.90–1.09 (m, 10.44H, cyclohexyl).

Tris-(4-(cyclohexylcarbonyl)-5-methyl-2-phenyl-2,4-dihydro-3H-pyrazol-3-onato) gallium (III), $[\text{Ga}(\text{Q}^{\text{CH}})_3](4)$

Slightly yellow powder: yield is 0.361 g (78%). Anal. calcd. for $\text{C}_{51}\text{H}_{57}\text{GaN}_6\text{O}_6$ (919.76): C, 66.60; H, 6.25; N, 9.14; Ga, 7.58; found: C, 66.64; H, 6.19; N, 9.21; Ga, 7.69%. IR: 3062 s; 2929 m ν_{as} CH (cyclohexyl); 2855 w ν_s CH (cyclohexyl); 2663 w; 2525 w; 2353 w; 1942 w; 1868 w; 1792 vs; 1606 vs. $\nu(\text{C}=\text{O})$; 1594 vs. $\nu(\text{C}=\text{C}, \text{C}=\text{N})$; 1579 s; 1535 vs; 1495 s $\nu(\text{C}=\text{C}, \text{C}=\text{N})$; 1463 s; 1437 m; 1411 s; 1386 m; 1363 m; 1351 m; 1325 w; 1242 w; 1177 w; 1140 w; 1124 s; 1079 m; 1066 m; 1027 m; 1010 m; 984 s $\delta_r(\text{C}-\text{H}$ cyclohexyl); 924 w; 907 w; 894 w; 872 w; 843 m; 818 m; 791 w; 768 m; 758 s; 716 w; 690 m; 659 m; 643 w; 625 m; 614 w; 509 w; 476 w; 448 w. $^1\text{H-NMR}$ (acetone- d_6): 8.00–7.78 (m, 2H, o- C_6H_5); 7.39 (t, 1.04H, p- C_6H_5); 7.26–7.12 (m, 2.03H, m- C_6H_5); 3.09 (m, 1.02H, HC-C=O); 2.48 (m, 3.12H, CH_3), 1.90–1.09 (m, 10.32H, cyclohexyl).

Polymeric tris-(4-(cyclohexylcarbonyl)-5-methyl-2-phenyl-2,4-dihydro-3H-pyrazol-3-onato) (aqua) scandium (III), $[\text{Sc}(\text{Q}^{\text{CH}})_3(\text{H}_2\text{O})]_n$ (5)

Ligand HQ^{CH} (1) (0.426 g, 1.5 mmol) was dissolved in 10 mL of EtOH (96%) at 45 °C and 0.5 mL (0.5 mmol) of 1 M aqueous $\text{Sc}(\text{ClO}_4)_3$ solution was added, followed by slow addition of 1.5 mL (1.5 mmol) of 1 M ethanolic NaOH solution. Light gray precipitate formed immediately, and the resulting thick suspension was stirred at 45 °C for 5 h and cooled to room temperature. The precipitate was filtered off, washed successively with 10 mL of 50% aqueous EtOH, 20 mL of deionized water, and 10 mL of hexane, and dried at 40 °C and 0.1 torr to a constant weight.

Light gray powder: yield is 0.424 g (93%). Anal. calcd. for $\text{C}_{51}\text{H}_{59}\text{N}_6\text{O}_7\text{Sc}$ (913.01): C, 67.09; H, 6.51; N, 9.20; Sc, 4.92; found: C, 67.15; H, 6.58; N, 9.15; Sc, 5.04%. IR: 3059 m; 2930 s ν_{as} CH (cyclohexyl); 2849 m ν_s CH (cyclohexyl); 1937 w; 1864 w; 1655 m $\delta(\text{H}_2\text{O})$; 1616 vs. $\nu(\text{C}=\text{O})$; 1595 s $\nu(\text{C}=\text{C}, \text{C}=\text{N})$; 1582 s; 1533 s; 1501 s; 1486 s $\nu(\text{C}=\text{C}, \text{C}=\text{N})$; 1464 m; 1451 s; 1440 s; 1402 m; 1382 m; 1350 m; 1326 w; 1269 w; 1239 w; 1210 w; 1178 w; 1130 w; 1114 w; 1082 m; 1030 w; 1011 w; 1000 w; 981 m $\delta_r(\text{C}-\text{H}$ cyclohexyl); 944 vw; 936 vw; 922 w; 904 w; 892 w; 869 vw; 842 w; 814 w; 793 w; 768 w; 753 m; 730 vw; 709 w; 689 w; 668 vw; 657 w; 643 w; 623 w; 614 w; 598 vw; 591 vw; 583 vw; 576 vw; 568 vw; 561 vw; 554 vw; 546 vw; 538 vw; 510 w; 502 w; 452 w; 431 w; 411 w; 403 w. $^1\text{H-NMR}$ (acetone- d_6): 7.98–7.94 (m, 2H, o- C_6H_5); 7.39–7.30 (m, 1.97H, m- C_6H_5); 7.23–7.15 (m, 0.96H, p- C_6H_5); 3.12 (m, 1.19H, HC-C=O); 2.45 (m, 3.27H, CH_3), 1.90–1.09 (m, 11.45H, cyclohexyl).

Synthesis of $[\text{La}(\text{Q}^{\text{CH}})_3(\text{H}_2\text{O})(\text{EtOH})]$ (7), $[\text{Gd}(\text{Q}^{\text{CH}})_3(\text{H}_2\text{O})]$ (8), and $[\text{Lu}(\text{Q}^{\text{CH}})_3(\text{H}_2\text{O})]$ (9)

Ligand HQ^{CH} (1) (0.341 g, 1.2 mmol) was dissolved in 10 mL of EtOH (96%) at 45 °C and 1.2 mL of 1 M ethanolic NaOH solution (1.2 mmol) was added dropwise with vigorous magnetic stirring. The pH of resulting solution was checked by universal indicator: it was almost neutral (pH~7), and the solution was stirred for additional 5 min. Then, the solution of corresponding hydrated chloride (0.4 mmol, 0.149 g of $\text{LaCl}_3 \cdot 7\text{H}_2\text{O}$, 0.149 g of $\text{GdCl}_3 \cdot 6\text{H}_2\text{O}$, or 0.156 g of $\text{LuCl}_3 \cdot 6\text{H}_2\text{O}$) in 3 mL of hot EtOH was slowly added and the mixture was stirred in a closed vial for additional 3 h at 45 °C. The solution become cloudy and heavy precipitate gradually formed. The suspension was cooled and the precipitate was filtered off, washed successively with 10 mL of 50% aqueous EtOH, 10 mL of deionized water, and 10 mL of hexane, and dried at 40 °C and 0.1 torr to a constant weight.

Tris-(4-(cyclohexylcarbonyl)-5-methyl-2-phenyl-2,4-dihydro-3H-pyrazol-3-onato) (aqua) (ethanol) lanthanum (III), $[\text{La}(\text{Q}^{\text{CH}})_3(\text{H}_2\text{O})(\text{EtOH})]$ (7)

White powder. Yield is 0.282 g (67%). Anal. calcd. for $\text{C}_{53}\text{H}_{65}\text{LaN}_6\text{O}_8$ (1053.02): C, 60.45; H, 6.22; N, 7.98; La, 13.19; found: C, 60.53; H, 6.29; N, 8.11; La, 13.27%. IR: 3654 vw;

3421 w ν_s H₂O; 2929 m ν_{as} CH (cyclohexyl); 2853 w ν_s CH (cyclohexyl); 1626 vs. ν (C=O); 1610 s; 1594 s ν (C=C, C=N); 1582 s; 1529 m; 1490 vs. ν (C=C, C=N); 1455 s; 1438 s; 1412 w; 1398 m; 1377 m; 1347 w; 1341 w; 1143 vw; 1099 vw; 1077 m; 1026 w; 1013 w; 980 m δ_r (C-H cyclohexyl); 940 vw; 894 vw; 810 w; 792 w; 761 m; 693 w; 671 w; 654 w; 621 w; 613 w; 511 vw; 497 vw; 449 vw. ¹H-NMR (acetone-d₆): 8.13–8.06 (m, 2H, o-C₆H₅); 7.32–7.18 (m, 1.97H, m-C₆H₅); 7.16–6.97 (m, 0.96H, p-C₆H₅); 2.93 (m, 1.31H, HC-C=O); 2.35 (m, 3.44H, CH₃), 1.81–1.06 (m, 11.79H, cyclohexyl).

Tris-(4-(cyclohexylcarbonyl)-5-methyl-2-phenyl-2,4-dihydro-3H-pyrazol-3-onato) (aqua) gadolinium (III), [Gd(Q^{CH})₃(H₂O)](8)

White powder. Yield is 0.301 g (73%). Anal. calcd. for C₅₁H₅₉GdN₆O₇ (1025.30): C, 59.74, H, 5.80, N, 8.20, Gd, 15.34; found: C, 60.07, H, 5.85, N, 8.33, Gd, 15.49%. IR: 3060 m; 2930 s ν_{as} CH (cyclohexyl); 2852 m ν_s CH (cyclohexyl); 2669 w; 1934 vw; 1874 vw; 1805 vw; 1649 s ν (H₂O); 1612 vs. ν (C=O); 1594 vs. ν (C=C, C=N); 1582 s; 1533 s; 1499 vs. ν (C=C, C=N); 1483 vs. ν (C=C, C=N); 1463 s; 1452 s; 1439 s; 1400 m; 1375 s; 1350 m; 1325 m; 1236 w; 1203 vw; 1176 w; 1130 w; 1080 s; 1028 m; 1011 m; 1000 w; 980 s δ_r (C-H cyclohexyl); 922 vw; 903 w; 892 w; 868 vw; 844 w; 812 m; 792 w; 768 m; 754 m; 704 w; 689 m; 655 m; 643 w; 621 m; 614 w; 533 vw; 509 w; 497 w; 449 w; 417 w.

Tris-(4-(cyclohexylcarbonyl)-5-methyl-2-phenyl-2,4-dihydro-3H-pyrazol-3-onato) (aqua) lutetium (III), [Lu(Q^{CH})₃(H₂O)](9)

White powder. Yield is 0.329 g (78%). Anal. calcd. for C₅₁H₅₉LuN₆O₇ (1043.03): C, 58.73, H, 5.70; N, 8.06; Lu, 16.78; found: C, 58.81, H, 5.76; N, 8.14%; Lu, 16.91%. IR: 3437 vw ν_s H₂O; 3060 vw; 2930 m ν_{as} CH (cyclohexyl); 2852 w ν_s CH (cyclohexyl); 2794 vw; 2668 vw; 1936 vw; 1653 m δ (H₂O); 1615 vs. ν (C=O); 1595 s; ν (C=C, C=N) 1583 m; 1534 m; 1501 s ν (C=C, C=N); 1486 s; 1464 m; 1451 m; 1440 m; 1401 w; 1379 m; 1349 vw; 1325 vw; 1238 vw; 1177 vw; 1131 vw; 1082 m; 1029 w; 1012 w; 999 vw; 981 m δ_r (C-H cyclohexyl); 922 vw; 905 vw; 892 vw; 844 vw; 814 w; 792 w; 783 vw; 769 w; 753 m; 707 vw; 700 vw; 689 w; 668 vw; 656 w; 644 vw; 622 w; 615 w; 509 w; 501 vw; 450 w; 425 vw; 420 vw. ¹H-NMR (DMSO-d₆): 8.57–8.51 (m, 2H, o-C₆H₅); 7.78–7.62 (m, 2.05H, m-C₆H₅); 7.55–7.44 (m, 1.04H, p-C₆H₅); 3.38 (m, 1.02H, HC-C=O); 2.80 (m, 3.03H, CH₃), 2.27–1.53 (m, 11.12H, cyclohexyl).

5. Conclusions

The influence of the type of central ion on the photophysical properties of the HQ^{CH} ligand was thoroughly investigated. We found that coordinating the HQ^{CH} by different trivalent metal ions increased the energies of both the first excited singlet and triplet states by 1500 cm⁻¹, except for the [Sc(Q^{CH})₃(H₂O)]_n complex, which showed a triplet increase of 600 cm⁻¹. However, the singlet–triplet energy gap slightly oscillated around 3900 cm⁻¹ for all the compounds. According to the Fermi golden rule, the intersystem crossing rate (k_{isc}) is proportional to the square of the energy transfer matrix element and inversely proportional to the energy gap. However, replacement of the Al³⁺ ion by a heavier one, such as Ga³⁺ or In³⁺, increased k_{isc} from 6.3×10^7 s⁻¹ to 8.9×10^7 s⁻¹. Notably, [Gd(Q^{CH})₃(H₂O)] was the only complex that demonstrated room temperature phosphorescence with approximately the same k_{isc} rate as HQ^{CH}. Therefore, we conclude that this phenomenon is not related to spin–orbit coupling enhancement, but rather to the paramagnetic properties of Gd³⁺ ion.

In this study, we demonstrated that HQ^{CH} predominantly emits from the T₁ state (phosphorescence). Trivalent metal ions fully suppress the ligand's phosphorescence, except for Gd, which is due to the paramagnetic properties of the Gd³⁺ ion.

We observed a significant increase in the quantum yield values up to 39 times for the complexes in comparison with HQ^{CH}. We established that the coordination compounds of lanthanide ions have the highest photoluminescence efficiencies, which are 19.5% for [La(Q^{CH})₃(H₂O)(EtOH)] and 19.0% for [Gd(Q^{CH})₃(H₂O)].

Thus, this paper shows that the nature of the non-luminescent cation has a dramatic effect on the luminescence features of acylpyrazolonate complexes. By varying the cation, one can control the nature of the emission, the energies of the singlet and triplet states, and

the lifetime of the excited states. The regularities shown in this work will be useful for the design of a new generation of WOLED devices.

Supplementary Materials: The supporting information can be downloaded at <https://www.mdpi.com/article/10.3390/ijms24098131/s1>.

Author Contributions: T.P.: methodology, writing—original draft, investigation. V.K.: conceptualization, methodology, writing—original draft, investigation. V.G.: investigation, writing. M.K.: investigation. Y.B.: investigation. C.P.: methodology, Writing—Original draft. I.T.: Conceptualization, investigation, writing—original draft, resources, project administration, funding acquisition. All authors have read and agreed to the published version of the manuscript.

Funding: The work was supported by the Russian Science Foundation under project #19-13-00272.

Institutional Review Board Statement: Not applicable.

Informed Consent Statement: Not applicable.

Data Availability Statement: Data available upon request.

Conflicts of Interest: The authors declare no conflict of interest.

References

1. Kido, J.; Kimura, M.; Nagai, K. Multilayer White Light-Emitting Organic Electroluminescent Device. *Science* **1995**, *267*, 1332–1334. [[CrossRef](#)] [[PubMed](#)]
2. D'Andrade, B.W.; Thompson, M.E.; Forrest, S.R. Controlling Exciton Diffusion in Multilayer White Phosphorescent Organic Light Emitting Devices. *Adv. Mater.* **2002**, *14*, 147–151. [[CrossRef](#)]
3. Zhou, N.; Wang, S.; Xiao, Y.; Li, X. Double light-emitting layer implementing three-color emission: Using DCJTb lightly doping in Alq3 as red-green emitting layer and APEAn1N as blue-green emitting layer. *J. Lumin.* **2018**, *196*, 40–49. [[CrossRef](#)]
4. Miao, Y.; Du, X.; Wang, H.; Liu, H.; Jia, H.; Xu, B.; Hao, Y.; Liu, X.; Li, W.; Huang, W. Simplified phosphorescent organic light-emitting devices using heavy doping with an Ir complex as an emitter. *RSC Adv.* **2015**, *5*, 4261–4265. [[CrossRef](#)]
5. Taidakov, I.; Ambrozevich, S.; Saifutyarov, R.; Lyssenko, K.; Avetisov, R.; Mozhevitina, E.; Khomyakov, A.; Khrizanforov, M.; Budnikova, Y.; Avetisov, I. New Pt(II) complex with extra pure green emission for OLED application: Synthesis, crystal structure and spectral properties. *J. Organomet. Chem.* **2018**, *867*, 253–260. [[CrossRef](#)]
6. Li, G.; Congrave, D.G.; Zhu, D.; Su, Z.; Bryce, M.R. Recent advances in luminescent dinuclear iridium (III) complexes and their application in organic electroluminescent devices. *Polyhedron* **2018**, *140*, 146–157. [[CrossRef](#)]
7. Hackney, H.E.; Perepichka, D.F. Recent advances in room temperature phosphorescence of crystalline boron containing organic compounds: Nanoscience: Special Issue Dedicated to Professor Paul S. Weiss. *Aggregate* **2022**, *3*, e123. [[CrossRef](#)]
8. Gierschner, J.; Shi, J.; Milián-Medina, B.; Roca-Sanjuán, D.; Varghese, S.; Park, S. Luminescence in Crystalline Organic Materials: From Molecules to Molecular Solids. *Adv. Opt. Mater.* **2021**, *9*, 2002251. [[CrossRef](#)]
9. Ma, K.; Chen, W.; Jiao, T.; Jin, X.; Sang, Y.; Yang, D.; Zhou, J.; Liu, M.; Duan, P. Boosting the circularly polarized luminescence of small organic molecules *via* multi-dimensional morphology control. *Chem. Sci.* **2019**, *10*, 6821–6827. [[CrossRef](#)]
10. Metlin, M.T.; Goryachii, D.O.; Aminev, D.F.; Datskevich, N.P.; Korshunov, V.M.; Metlina, D.A.; Pavlov, A.A.; Mikhailchenko, L.V.; Kiskin, M.A.; Garaeva, V.V.; et al. Bright Yb³⁺ complexes for efficient pure near-infrared OLEDs. *Dye. Pigment.* **2021**, *195*, 109701. [[CrossRef](#)]
11. Korshunov, V.M.; Ambrozevich, S.A.; Taydakov, I.V.; Vashchenko, A.A.; Goriachiy, D.O.; Selyukov, A.S.; Dmitrienko, A.O. Novel β -diketonate complexes of Eu³⁺ bearing pyrazole moiety for bright photo- and electroluminescence. *Dye. Pigment.* **2019**, *163*, 291–299. [[CrossRef](#)]
12. Wu, K.; Zhang, T.; Wang, Z.; Wang, L.; Zhan, L.; Gong, S.; Zhong, C.; Lu, Z.-H.; Zhang, S.; Yang, C. De Novo Design of Excited-State Intramolecular Proton Transfer Emitters via a Thermally Activated Delayed Fluorescence Channel. *J. Am. Chem. Soc.* **2018**, *140*, 8877–8886. [[CrossRef](#)]
13. Vitukhnovsky, A.G.; Ambrozevich, S.A.; Korshunov, V.M.; Taydakov, I.V.; Metlin, M.T.; Selyukov, A.S. Effect of Bonding Scandium (III) ion to 1,3-Diketones on Their Luminescent Properties. *J. Russ. Laser Res.* **2018**, *39*, 165–169. [[CrossRef](#)]
14. Verma, P.K.; Steinbacher, A.; Koch, F.; Nuernberger, P.; Brixner, T. Monitoring ultrafast intramolecular proton transfer processes in an unsymmetric β -diketone. *Phys. Chem. Chem. Phys.* **2015**, *17*, 8459–8466. [[CrossRef](#)] [[PubMed](#)]
15. Vitukhnovsky, A.G.; Ambrozevich, S.A.; Korshunov, V.M.; Taydakov, I.V.; Lyssenko, K.A.; Metlin, M.T.; Selyukov, A.S. Luminescent properties of complexes based on scandium (III) β -diketonates. *J. Lumin.* **2018**, *201*, 509–519. [[CrossRef](#)]
16. Thejokalyani, N.; Dhoble, S.J. Novel approaches for energy efficient solid state lighting by RGB organic light emitting diodes—A review. *Renew. Sustain. Energy Rev.* **2014**, *32*, 448–467. [[CrossRef](#)]
17. Zinna, F.; Pasini, M.; Galeotti, F.; Botta, C.; Di Bari, L.; Giovanella, U. Design of Lanthanide-Based OLEDs with Remarkable Circularly Polarized Electroluminescence. *Adv. Funct. Mater.* **2017**, *27*, 1603719. [[CrossRef](#)]

18. Bochkov, M.A.; Vitukhnovsky, A.G.; Taidakov, I.V.; Vashchenko, A.A.; Katsaba, A.V.; Ambrozevich, S.A.; Brunkov, P.N. Optimization of carrier mobility in luminescence layers based on europium β -diketonates in hybrid light-emitting structures. *Semiconductors* **2014**, *48*, 369–372. [[CrossRef](#)]
19. Nehra, K.; Dalal, A.; Hooda, A.; Bhagwan, S.; Saini, R.K.; Mari, B.; Kumar, S.; Singh, D. Lanthanides β -diketonate complexes as energy-efficient emissive materials: A review. *J. Mol. Struct.* **2022**, *1249*, 131531. [[CrossRef](#)]
20. Binnemans, K. Lanthanide-Based Luminescent Hybrid Materials. *Chem. Rev.* **2009**, *109*, 4283–4374. [[CrossRef](#)]
21. Ho, C.-L.; Wong, W.-Y. Metal-containing polymers: Facile tuning of photophysical traits and emerging applications in organic electronics and photonics. *Coord. Chem. Rev.* **2011**, *255*, 2469–2502. [[CrossRef](#)]
22. Carlotto, S.; Babetto, L.; Bortolus, M.; Carlotto, A.; Rancan, M.; Bottaro, G.; Armelao, L.; Carbonera, D.; Casarin, M. Nature of the Ligand-Centered Triplet State in Gd^{3+} β -Diketonate Complexes as Revealed by Time-Resolved EPR Spectroscopy and DFT Calculations. *Inorg. Chem.* **2021**, *60*, 15141–15150. [[CrossRef](#)] [[PubMed](#)]
23. Kitagawa, Y.; Tsurui, M.; Hasegawa, Y. Bright red emission with high color purity from Eu (III) complexes with π -conjugated polycyclic aromatic ligands and their sensing applications. *RSC Adv.* **2022**, *12*, 810–821. [[CrossRef](#)] [[PubMed](#)]
24. Korshunov, V.M.; Tsoarieva, A.V.; Gontcharenko, V.E.; Zanizdra, S.R.; Metlin, M.T.; Polikovskiy, T.A.; Taydakov, I.V. Photophysical Properties of Eu^{3+} β -Diketonates with Extended π -Conjugation in the Aromatic Moiety. *Inorganics* **2022**, *11*, 15. [[CrossRef](#)]
25. Balzani, V.; Ceroni, P.; Juris, A. *Photochemistry and Photophysics: Concepts, Research, Applications*; Wiley-VCH: Weinheim, Germany, 2014; ISBN 978-3-527-33479-7.
26. Marchetti, F.; Pettinari, C.; Pettinari, R. Acylpyrazolone ligands: Synthesis, structures, metal coordination chemistry and applications. *Coord. Chem. Rev.* **2005**, *249*, 2909–2945. [[CrossRef](#)]
27. Belousov, Y.A.; Drozdov, A.A. Lanthanide acylpyrazolonates: Synthesis, properties and structural features. *Russ. Chem. Rev.* **2012**, *81*, 1159–1169. [[CrossRef](#)]
28. Marchetti, F.; Pettinari, R.; Pettinari, C. Recent advances in acylpyrazolone metal complexes and their potential applications. *Coord. Chem. Rev.* **2015**, *303*, 1–31. [[CrossRef](#)]
29. Taydakov, I.V.; Belousov, Y.A.; Lyssenko, K.A.; Varaksina, E.; Drozdov, A.A.; Marchetti, F.; Pettinari, R.; Pettinari, C. Synthesis, phosphorescence and luminescence properties of novel europium and gadolinium tris-acylpyrazolonate complexes. *Inorganica. Chim. Acta* **2020**, *502*, 119279. [[CrossRef](#)]
30. Zhang, D.; Shi, M.; Liu, Z.; Li, F.; Yi, T.; Huang, C. Luminescence Modulation of a Terbium Complex with Anions and Its Application as a Reagent. *Eur. J. Inorg. Chem.* **2006**, *2006*, 2277–2284. [[CrossRef](#)]
31. Xin, H.; Shi, M.; Gao, X.C.; Huang, Y.Y.; Gong, Z.L.; Nie, D.B.; Cao, H.; Bian, Z.Q.; Li, F.Y.; Huang, C.H. The Effect of Different Neutral Ligands on Photoluminescence and Electroluminescence Properties of Ternary Terbium Complexes. *J. Phys. Chem. B* **2004**, *108*, 10796–10800. [[CrossRef](#)]
32. Shen, L.; Shi, M.; Li, F.; Zhang, D.; Li, X.; Shi, E.; Yi, T.; Du, Y.; Huang, C. Polyaryl Ether Dendrimer with a 4-Phenylacetyl-5-pyrazolone-based Terbium (III) Complex as Core: Synthesis and Photophysical Properties. *Inorg. Chem.* **2006**, *45*, 6188–6197. [[CrossRef](#)]
33. Liu, J.; Shi, Q.; He, Y.; Fu, G.; Li, W.; Miao, T.; Lü, X. Single-molecule white-light of tris-pyrazolonate- Dy^{3+} complexes. *Inorg. Chem. Commun.* **2019**, *109*, 107573. [[CrossRef](#)]
34. Li, X.-L.; Li, J.; Zhu, C.; Han, B.; Liu, Y.; Yin, Z.; Li, F.; Liu, C.-M. An intense luminescent Dy (III) single-ion magnet with the acylpyrazolonate ligand showing two slow magnetic relaxation processes. *New J. Chem.* **2018**, *42*, 16992–16998. [[CrossRef](#)]
35. Zhang, Z.; Yu, C.; Liu, L.; Li, H.; He, Y.; Lü, X.; Wong, W.-K.; Jones, R.A. Efficient near-infrared (NIR) luminescent PMMA-supported hybrid materials doped with tris- β -diketonate Ln^{3+} complex ($Ln = Nd$ or Yb). *J. Photochem. Photobiol. Chem.* **2016**, *314*, 104–113. [[CrossRef](#)]
36. Pettinari, C.; Marchetti, F.; Pettinari, R.; Drozdov, A.; Troyanov, S.; Voloshin, A.I.; Shavaleev, N.M. Synthesis, structure and luminescence properties of new rare earth metal complexes with 1-phenyl-3-methyl-4-acylpyrazol-5-ones. *J. Chem. Soc. Dalton Trans.* **2002**, 1409–1415. [[CrossRef](#)]
37. Bünzli, J.-C.G.; Eliseeva, S.V. Basics of Lanthanide Photophysics. In *Lanthanide Luminescence*; Hänninen, P., Härmä, H., Eds.; Springer Series on Fluorescence; Springer: Berlin/Heidelberg, Germany, 2010; Volume 7, pp. 1–45. ISBN 978-3-642-21022-8.
38. Berrones-Reyes, J.C.; Vidyasagar, C.C.; Muñoz Flores, B.M.; Jiménez-Pérez, V.M. Luminescent molecules of main group elements: Recent advances on synthesis, properties and their application on fluorescent bioimaging (FBI). *J. Lumin.* **2018**, *195*, 290–313. [[CrossRef](#)]
39. Lewis, G.N.; Kasha, M. Phosphorescence and the Triplet State. *J. Am. Chem. Soc.* **1944**, *66*, 2100–2116. [[CrossRef](#)]
40. Johnson, D.W.; Xu, J.; Saalfrank, R.W.; Raymond, K.N. Self-Assembly of a Three-Dimensional $[Ga_6(L^2)_6]$ Metal-Ligand “Cylinder”. *Angew. Chem. Int. Ed.* **1999**, *38*, 2882–2885. [[CrossRef](#)]
41. Singh, D.; Nishal, V.; Bhagwan, S.; Saini, R.K.; Singh, I. Electroluminescent materials: Metal complexes of 8-hydroxyquinoline—A review. *Mater. Des.* **2018**, *156*, 215–228. [[CrossRef](#)]
42. Belousov, Y.A.; Korshunov, V.M.; Metlin, M.T.; Metlina, D.A.; Kiskin, M.A.; Aminev, D.F.; Datskevich, N.P.; Drozdov, A.A.; Pettinari, C.; Marchetti, F.; et al. Towards bright dysprosium emitters: Single and combined effects of environmental symmetry, deuteration, and gadolinium dilution. *Dye. Pigment.* **2022**, *199*, 110078. [[CrossRef](#)]

43. Belousov, Y.A.; Metlin, M.T.; Metlina, D.A.; Kiskin, M.A.; Yakushev, I.A.; Polikovskiy, T.A.; Taydakov, I.V.; Drozdov, A.A.; Marchetti, F.; Pettinari, C. Self-Assembly of a Two-Dimensional Coordination Polymer Based on Silver and Lanthanide Tetrakis-Acylpyrazolonates: An Efficient New Strategy for Suppressing Ligand-to-Metal Charge Transfer Quenching of Europium Luminescence. *Polymers* **2023**, *15*, 867. [[CrossRef](#)] [[PubMed](#)]
44. Jou, J.-H.; Hsieh, C.-Y.; Tseng, J.-R.; Peng, S.-H.; Jou, Y.-C.; Hong, J.H.; Shen, S.-M.; Tang, M.-C.; Chen, P.-C.; Lin, C.-H. Candle Light-Style Organic Light-Emitting Diodes. *Adv. Funct. Mater.* **2013**, *23*, 2750–2757. [[CrossRef](#)]
45. Singh, Y.P.; Rai, A.K. Synthesis and Characterisation of 4-Acyl-3-methyl-2-pyrazolin-5-one Complexes of Aluminium. *Synth. React. Inorg. Met.-Org. Chem.* **1982**, *12*, 85–102. [[CrossRef](#)]
46. Bhomia, J.; Sharma, J.; Singh, Y. Synthesis and characterization of asymmetric dinuclear aluminum compounds containing sterically hindered heterocyclic β -diketones. *Main Group Met. Chem.* **2016**, *39*, 151–155. [[CrossRef](#)]
47. Okafor, E.C. The Metal Complexes of Heterocyclic β -Diketones and their Derivatives, Part VIII Synthesis, Structure, Proton NMR and Infrared Spectral Studies of the Complexes of Al (III), Fe (III), Co (III), Rh (III), In (III), and Zr (IV) with 1-Phenyl-3-methyl-4-trifluoroacetyl-pyrazolone-5 (HPMTFP). *Z. Nat. B* **1981**, *36*, 213–217. [[CrossRef](#)]
48. Tayeb, A.; Goetz-Grandmont, G.J.; Brunette, J.P. Analytical and spectroscopic study of indium extraction with 1,10-Bis(1-phenyl-3-methyl-5-hydroxy-4-pyrazolyl)-1,10-decanedione and its mixtures with Tri-n-octylphosphine oxide. *Mon. Chem.* **1991**, *122*, 453–466. [[CrossRef](#)]
49. Morales, R.; Nekimken, H.; Bartholdi, C.S.; Cunningham, P.T. Spectral studies of heterocyclic β -diketonates of actinide, lanthanide, and transition metals. *Spectrochim. Acta Part Mol. Spectrosc.* **1988**, *44*, 165–169. [[CrossRef](#)]
50. Akama, Y.; Sawada, T.; Ueda, T. Thermal and spectroscopic studies of scandium complex of 1-phenyl-3-methyl-4-benzoyl-5-pyrazolone. *J. Mol. Struct.* **2005**, *750*, 44–50. [[CrossRef](#)]
51. Pettinari, C.; Marchetti, F.; Pettinari, R.; Natanti, P.; Drozdov, A.; Semenov, S.; Troyanov, S.I.; Zolin, V. Syntheses, spectroscopic characterization and X-ray structural studies of lanthanide complexes with adamantyl substituted 4-acylpyrazol-5-one. *Inorg. Chim. Acta* **2006**, *359*, 4063–4070. [[CrossRef](#)]
52. Pettinari, C.; Marchetti, F.; Pettinari, R.; Drozdov, A.; Semenov, S.; Troyanov, S.I.; Zolin, V. A new rare-earth metal acylpyrazolonate containing the Zundel ion stabilized by strong hydrogen bonding. *Inorg. Chem. Commun.* **2006**, *9*, 634–637. [[CrossRef](#)]
53. Wasserberg, D. (*Dorothee*) *Triplet States—Triplet Fates: Phosphorescence and Energy Transfer in Functional Molecules*; Technische Universiteit Eindhoven: Eindhoven, The Netherlands, 2006. [[CrossRef](#)]
54. Xiong, Y.; Zhao, Z.; Zhao, W.; Ma, H.; Peng, Q.; He, Z.; Zhang, X.; Chen, Y.; He, X.; Lam, J.W.Y.; et al. Designing Efficient and Ultralong Pure Organic Room-Temperature Phosphorescent Materials by Structural Isomerism. *Angew. Chem.* **2018**, *130*, 8129–8133. [[CrossRef](#)]
55. Hamzehpoor, E.; Peregichka, D.F. Crystal Engineering of Room Temperature Phosphorescence in Organic Solids. *Angew. Chem.* **2020**, *132*, 10063–10067. [[CrossRef](#)]
56. Sheldrick, G.M. Crystal structure refinement with SHELXL. *Acta. Crystallogr. Sect. C Struct. Chem.* **2015**, *C71*, 3–8. [[CrossRef](#)]
57. Sheldrick, G.M. SHELXT—Integrated space-group and crystal-structure determination. *Acta. Crystallogr. Sect. Found. Adv.* **2015**, *A71*, 3–8. [[CrossRef](#)] [[PubMed](#)]
58. Dolomanov, O.V.; Bourhis, L.J.; Gildea, R.J.; Howard, J.A.K.; Puschmann, H. OLEX2: A complete structure solution, refinement and analysis program. *J. Appl. Crystallogr.* **2009**, *42*, 339–341. [[CrossRef](#)]

Disclaimer/Publisher’s Note: The statements, opinions and data contained in all publications are solely those of the individual author(s) and contributor(s) and not of MDPI and/or the editor(s). MDPI and/or the editor(s) disclaim responsibility for any injury to people or property resulting from any ideas, methods, instructions or products referred to in the content.